A STUDY ON THz COMMUNICATIONS BETWEEN LOW EARTH ORBIT CONSTELLATIONS AND EARTH STATIONS

Estephania Flores Aguilar[1] and Gunes Karabulut-Kurt[1]
[1]Polytechnique Montréal, 2500 Chem. de Polytechnique, Montréal, QC H3T 1J4, Canada

NOTE: Corresponding author: Estephania Flores, estephania.flores-aguilar@polymtl.ca

Abstract – *A non-terrestrial system that uses Terahertz (THz) frequencies is a potential solution to achieving equal access to the Internet worldwide. This paper describes a non-terrestrial system that consists of a Low Earth Orbit (LEO) constellation, Earth Stations in Motion (ESIMs) and standard Earth stations. We examine the effects of rain, fog, clouds and atmospheric gases for this non-terrestrial system for frequencies between 100-300 GHz. The research findings suggest that the frequency bands between 102 - 109.5 GHz are rather suitable for communication between Earth stations and satellites, including ESIMs, reaching in a critical scenario uplink data rates of up to 2.6 Gbits/s with 0.5 GHz of bandwidth or up to 12 Gbits/s with 5 GHz of bandwidth in uplink. For the downlink, we can reach up to 6 Mbits/s with a transmitted power of 29 dBW, but if we increase the power transmitted by satellites, it is possible to reach up to 25 Gbits/s with 2.5GHz of bandwidth. Under clear, blue-sky conditions, we can achieve a maximum data rate of 17.3 Gbits/s for downlink and uplink. For inter-satellite links (communications between satellites in the same orbit or between different orbits), the frequency bands between 111.8 – 114.25 GHz, 116 – 123 GHz, 174.5 – 182 GHz, 185 – 190 GHz are viable, offering speeds from 1.5 to 2.51 Gbits/s when using a uniform rectangular array with 625 radiating elements. This research provides new findings from the amalgamation of existing literature, which is crucial for the future allocation of optimal frequencies between 100 - 300 GHz for satellite services.*

Keywords – Atmospheric gases, attenuation, cloud, Earth stations in motion, fog, rain, terahertz

1. INTRODUCTION

1.1 Motivation and contribution

Despite the increasing need for connectivity and high demand for broadband in urban areas, many rural regions in most countries still lack Internet access. One of the reasons for these connectivity gaps is the high cost and low profitability of deploying terrestrial services, such as mobile or fixed networks, in these areas due to low demand. However, a potential solution to achieving equal access to the Internet worldwide is the use of non-terrestrial systems. These systems could be composed of mega-constellations of Non-Geostationary Satellites (NGSO) that offer several advantages. For example, they have low construction and launch costs, reduced latency and a large global footprint when integrated with satellites in Low Earth Orbits (LEOs).

In recent years, the first satellites of massive constellations of LEO satellites have been put in orbit. For example, in 2019 Oneweb, Amazon and SpaceX launched 650, 3 236 and 42 000 satellites, respectively [1].

In 2023 it was expected that 7500 additional satellites would be in orbit as part of the second generation of SpaceX's constellation "Starlink", for which the use of the Ka and Ku bands was already authorized by the Federal Communications Commission (FCC) of the Unites States, and the analysis of its operation in the E-band was postponed by this later [2]. Satellite building contracts have been given to manufacturers such as Viasat and Boeing, and they are actively building satellites. Telesat has also been given over 500M CAD by the Canadian government to build a Canadian network. Overall, governments worldwide are actively working on modernizing international regulations to enable and facilitate the provision of global connectivity by LEO mega-constellations.

Furthermore, the International Telecommunication Union (ITU) reports that the total number of NGSO satellite filings registered increased by around 65.6% between 2018 and 2022 (either in the Advance Publication Information (API), coordination or notification stage), having increased from 486 to 667 filings registered in the Master International Frequency Register [3].

In addition, the upcoming NGSO constellations will be able to provide services at fibre-like speeds, including to aircraft, ships and trains, with low latency experience in the frequencies allocated to the Fixed Satellite Service (FSS). There is also a trend towards convergence of Non-Terrestrial Networks (NTN) with the Mobile Satellite Service (MSS) and the terrestrial network (mobile service), such as in the case of SpaceX, whose Starlink satellites will be able to support frequencies around 2 GHz allocated to the MSS and will be connected with the T-Mobile network in 2023. Another example is Lynk Global, the first company to demonstrate the technical feasibility of sending a text message via satellite communications to unmodified mobile phones.

It should be noted that satellites operate in three main allocation services: FSS, MSS and Broadcasting Satellite

Service (BSS). According to the ITU Radio Regulations (RR), FSS refers to a radiocommunication service involving Earth stations at specific locations using one or more satellites. MSS is a radiocommunication service between mobile Earth stations and one or more satellites. Finally, BSS is a radiocommunication service where signals transmitted or retransmitted by satellites are intended for direct reception by the general public [4].

However, finding enough spectrum to enable widespread connectivity will be a challenge, particularly due to the increasing number of satellite systems operating in the geostationary orbit and NGSO, which commonly use frequencies below 30 GHz. This raises the likelihood of harmful interference between satellite services and makes international frequency coordination more difficult. To address this growing demand for spectrum, two main approaches are currently being explored: schemes to use spectrum more efficiently or expanding the use of spectrum to higher frequency bands to make more spectrum available. For example, using Terahertz (THz) frequencies, that according to [5] usually refer to the frequency band between 100 GHz and 3000 GHz.

Our work proposes to study the viability of using THz frequencies for LEO mega-constellation satellite communication, with a focus on frequencies between 100 GHz and 300 GHz, which have not yet been allocated to satellite services by the existing regulatory framework of the ITU. The attenuation factors including rain, based on the ITU-R P.838-3 model [6], fog and clouds, based on the ITU-R P.840 model [7], and the methodology used in [8], and atmospheric gases based on the ITU-R P.676-13 model [9], are considered. These models are accepted as international standards and provide guidelines and calculations based on extensive measurements.

We principally analyzed the frequencies between 100 GHz and 300 GHz because they have a tendency to be used in the future. For example, the ITU, the Asia-Pacific Telecommunity and countries such as Canada are working to facilitate new wireless technologies and services in these frequency bands. The ITU's Working Party 5D explored the possibilities of wireless communication in the 100-300 GHz range [10], and Canada published the Decision on the Technical and Policy Framework for the Frequency Bands Above 95 GHz in 2020 [11], aiming to enable companies to develop new use cases and enhance innovation. Additionally, the frequency segments of 230-255 GHz and others are under study by the ITU for the World Radio Conferences of 2023 [12] and 2027 [13].

This paper is organized as follows: In the following subsection, we provide an overview of the literature. The system model is given in Section 2. Section 3 focuses on the attenuation factors. Numerical results are given in Section 4. Regulatory aspects and project assessment are analyzed in sections 5 and 6, respectively. The conclusion and open issues are given in Section 7.

1.2 Related work

In order to determine the performance of the waves in the THz frequencies, it is necessary to understand the factors that affect signals, such as free space, rain, fog or atmospheric gases. In this regard, in Table 1, there is a review of the elements to be considered and the existing literature for THz frequencies.

In respect of the abbreviations in Table 1, ES to Sat stands for Earth station to satellite or satellite to the Earth station, ESIM to Sat means ESIM to satellite or satellite to ESIM, and ISL means inter-satellite links.

Additionally, in [21], the ionospheric fading for ISLs is studied. As a result, it is shown that the ionospheric plasma does not affect the ISL propagation in THz frequencies while satellites are in near-Earth orbits. However, the study of the Earth stations to satellite links is missing.

With respect to NGSO satellites, in 2019, an agreement was reached at the World Radiocommunications Conference (WRC) to establish regulatory procedures for the deployment of NGSO systems, including mega-constellations in LEO. As a result, Resolution 35 was published [22]. This was a significant step towards enabling the use of non-terrestrial systems for global connectivity.

Furthermore, the ITU is carrying out studies related to THz frequencies. For example, in 2023, as part of agenda item 1.14 of the WRC 2023, it was decided that the frequency ranges 239.2-242.2 GHz and 244.2-247.2 GHz are going to be allocated to the Earth Exploration Satellite Service (EESS) with passive sensors. [23]. However, it is important to note that the purpose and operations of this satellite service are different to satellites that target communication purposes. According to the ITU, *"the EESS passive sensors measure the natural noise floor, namely, the electromagnetic energy emitted, absorbed or scattered by the Earth's surface or atmosphere"*[24]. In addition, the ITU is also planning to carry out studies for the WRC 2027. Under agenda item 1.8, the ITU will consider possible additional primary allocations to the radiolocation service in the frequency range 231-275 GHz. Under agenda item 1.10, the ITU will consider limits for power flux density

Table 1 – Propagation effects in THz frequencies

Attenuation	**ES to Sat**	**ESIM to Sat**	**ISL**	**Literature**
Rain	Yes	No	No	[5], [14], [6]
Fog and cloud	Yes	Yes	No	[15], [16], [7], [8]
Atmospheric Gases	Yes	Yes	No	[5],[17], [18],[9], [19]
Free space	Yes	Yes	Yes	[18],[20], [19]

and equivalent isotropic radiated power for the FSS, MSS and BSS to protect fixed and mobile services in the frequency bands 71-76 GHz and 81-86 GHz (Earth-to-space) item and, under agenda item 1.18, the ITU will consider possible regulatory measures regarding the protection of the EESS (passive) and the radio astronomy service in certain frequency bands above 76 GHz from unwanted emissions of active services[25].

Despite the existing literature, there is a lack of extensive research on the effects of free space, rain, fog, atmospheric gases or ionospheric fading in non-terrestrial systems using THz frequencies. This highlights the need for further exploration of wave propagation in THz (100 to 300 GHz) frequencies and their potential use by non-terrestrial systems.

2. COMMUNICATION SYSTEM MODEL

2.1 Description of the non-terrestrial communication system

The model described in this document consists of three layers: the top, middle, and lower layers. The top layer is made up of a constellation of NGSO satellites that operate at altitudes between 200 km and 2000 km, using frequencies between 100 GHz and 300 GHz for communication. The middle layer consists of aeronautical ESIMs, which are facilities that provide fixed communications at aircraft in altitudes between 5.76 - 10.69 km. The lower layer is made up of standard Earth stations installed on Earth, which communicate with satellites in the upper layer. Fig. 1 shows the scheme of the non-terrestrial communication system that was previously described.

In Fig. 1, different types of links are represented by different symbols. H_{ES} represents the link from an Earth station to a satellite, while H_{SE} is the link from a satellite to an Earth station. H_{AS} means the link from an aeronautical ESIM to a satellite, while H_{SA} is the link from a satellite to an aeronautical ESIM. Finally, H_{SS} means satellite-to-satellite links.

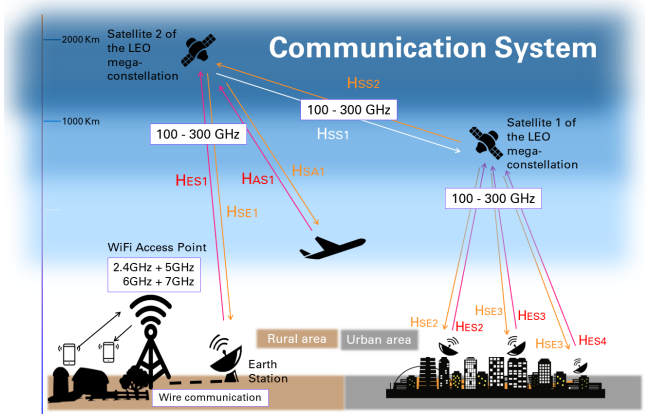

Fig. 1 – An overview of the considered communication system

Table 2 – Frequencies under study

Frequencies under study	
Nomenclature	Segment
Band-1	102 – 109.5 GHz
Band-2	111.8 - 114.25 GHz
Band-3	116 - 123 GHz
Band-4	131.5 – 148.5 GHz
Band-5	151.5 - 158.5 GHz
Band-6	174.5 – 182 GHz
Band-7	185 - 190 GHz
Band-8	226 – 232 GHz
Band-9	240 – 250 GHz
Band-10	252 - 300 GHz

2.2 Frequency bands

For this study, an analysis of the RR 2020 of the ITU was done in order to determine the frequency bands that are between 100 GHz and 300 GHz, and that globally are not yet allocated to FSS, MSS and BSS. Additionally, we considered note 5.340 of the RR of the ITU, which establishes that in some frequencies emissions are prohibited. From this analysis, the frequencies mentioned in Table 2 were obtained.

The hypothesis is that the frequency bands mentioned in Table 2 are viable and should be allocated to satellite services. With these new allocations, more spectrum is available globally to be used by LEO mega-constellations, providing less congested spectrum and bigger contiguous bandwidths, with the ability to support more LEO mega-constellations, as well as faster and easier international frequency coordination.

2.3 Main parameters and assumptions

The scenario that we consider was designed to receive and transmit signals from three different locations: Montreal, Mexico City and Manaos in Brazil. Therefore, it considers the typical environmental conditions of those cities for the month of March. We selected this month as it generally characterizes three distinct weather patterns found globally throughout the year. For instance, Montreal experiences cold and humid conditions in March, Mexico City is warm and dry, and Manaos is hot and humid.

In this context, Table 3 shows the main parameters used for the computations of this research.

Moreover, for the satellite's antenna gain (transmission and reception), we consider the values that we computed for a Uniform Rectangular phased Array (URA), which are shown in figures 3 and 4. We examined two URA structures: a rectangular lattice and a triangular lattice (see Fig. 2), with the objective of understanding the influence of the lattice structure on the number of grating lobes. Additionally, in our computations we increased the number of elements that form the URA, in order to under-

Table 3 – Main parameters

Description	Value
Altitude LEO satellites	h = 200 - 2000 km
Altitude aircraft	h_a =5.76 - 10.69 km
Elevation angle	θ = 30 Degrees
Earth radius	R_E = 6371 km
Speed of light	$c = 3 \times 10^8$ m/s
Power Tx- Earth station	P_{tx} = 56 dBW
Power Tx- satellite	p_{tx} = 29 dBW
Gain Tx- Earth station	G_{tx} = 80 dBi
Gain Rx- Earth station	G_{rx} = 68 dBi
Ambient temperature in fog or cloud	T_f = 273.15 K
Liquid water density	M = 0.5 g/m^3
Average temperature - Montreal (March)[26]	T_{MTL} = 283.15 K
Average temperature - Mexico City (March)[26]	T_{CDMX} = 296.15 K
Average temperature - Manaos (March)[26]	T_M = 304.15 K
Dry air pressure (Montreal, Mexico City, Manaos)	P= 1012, 778.1, 1010 hP
Water vapour density[27]	ρ = 7.5 g/m^3
Rain Rate - Montreal (0.01% of time)[28]	R_{MTL} = 28 mm/hr
Rain Rate - Mexico City (0.01% of time)[28]	R_{CDMX} = 63 mm/hr
Rain Rate - Manaos (0.01% of time)[28]	R_M = 90 mm/hr

stand its impact in the gain. From figures 3 and 4 we observe that the gain exhibits a pattern of horizontal peaks and troughs, each occurring within different bands. For instance, in Band-4, the rectangular lattice shows a decrease in the middle of the band, whereas the triangular lattice ascends to reach a peak.

Furthermore, we discern that both architectures exhibit identical gain values. The maximum gain values are observed for an array comprising 625 elements, which can attain up to 27.7 dBi. Conversely, the minimum values are associated with antennas consisting of 25 radiating elements, exhibiting values approximately between 10 dBi and 15 dBi. Thus, we can observe that the gain increases as the number of elements does. Our results are corroborated with article [29] where a comprehensive analysis of the phase array operating in THz frequencies is presented. According the article a circular planar self-complementary square spiral can reach up to 29 dB, and a self-complimentary sinuous directivity ranges between 24 dB and 32 dB.

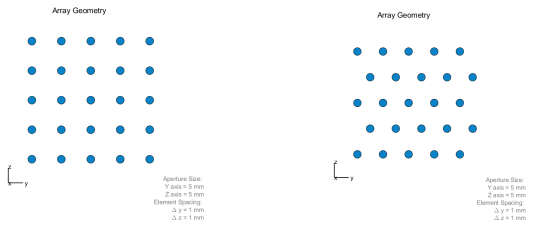

(a) *Rectangular lattice* **(b)** *Triangular lattice*

Fig. 2 – Uniform rectangular array

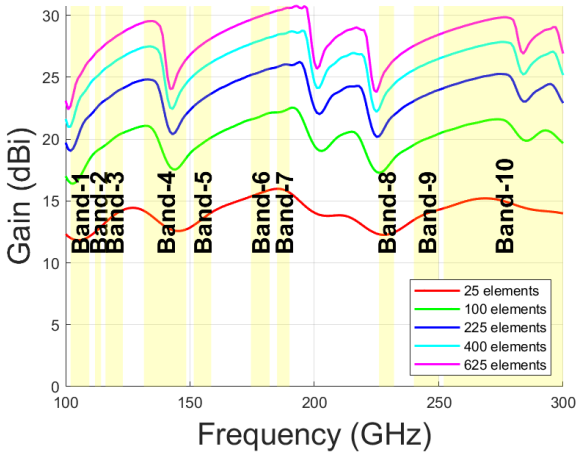

Fig. 3 – URA gain, rectangular lattice

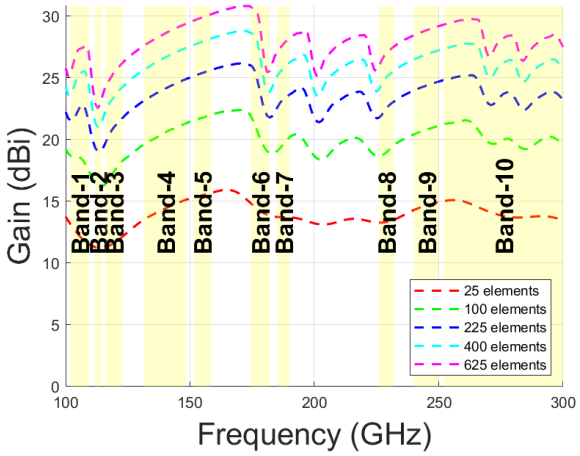

Fig. 4 – URA gain, triangular lattice

3. ATTENUATION OF SIGNAL PROPAGATION

As it was mentioned before, to determine the performance of our communication system, it is important to consider the path loss, l_p, which could be obtained from:

$$l_p = l_r + l_{fc} + l_g + l_f. \quad \text{(dB)} \qquad (1)$$

In this context, l_r represents the attenuation due to rain, l_{fc} denotes the attenuation caused by fog and clouds, l_g is the attenuation due to atmospheric gases, and l_f signifies the free space attenuation. For frequency bands below

1000 GHz, the calculation of l_p incorporates the methods and equations proposed in references [6], [7], [9] and [20] published by ITU. These methods are further reviewed in the subsequent subsections.

3.1 Rain attenuation

One of the factors that affect the performance of satellite communications is rain attenuation. The presence of raindrops along the path of signal propagation can cause a decrease in signal strength. In order to determine the rain attenuation, first, it is necessary to determine the rain height h_R, which is the maximum altitude where the signal can be attenuated by the rain. To compute h_R, we can use equations and values proposed in [30], described as follows:

$$h_R = h_0 + 0.36, \quad \text{(km)} \tag{2}$$

where h_0 is the 273.15 K (0ºC) isotherm height above mean sea level in km. For the Montreal area, it is $h_0 = 3$ km, for Mexico City around 4.9 km, and for Manaos around 6.59 km. Thus, the resulting rain height is around 3.36 km, 5.275 km and 6.953 km, respectively.

The second step involves calculating the slant range d_R. For elevation angles greater than 5º, the ITU recommends using equation *(3)*, where h_s represents the height of the Earth station above mean sea level in kilometers

$$d_R = \frac{(h_R - h_s)}{\sin\theta}. \quad \text{(km)} \tag{3}$$

To enhance understanding, a diagram is presented Fig. 5 that illustrates the altitude of the rain and the path followed by the signal. In this diagram, the elevation angle is represented by the symbol θ and is measured in degrees.

A third step is to obtain the horizontal projection of the slant range on the ground d_g in kilometers, using $d_g = d_R \cos\theta$. Furthermore, the rain attenuation γ_r in dB/km could be obtained from [6]:

$$\gamma_r = kR^{\alpha}, \quad \text{(dB/km)} \tag{4}$$

where R is the rain rate mentioned in Table 3, in millimeters per hour for each city. k and α are coefficients that depend on the frequency, the polarization state, and the elevation angle of the signal path [6]. They could be

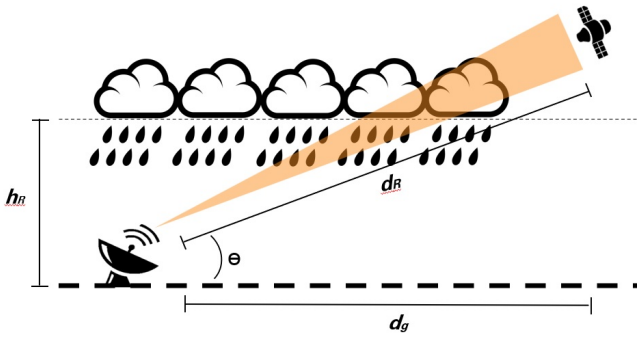

Fig. 5 – Rain schema

obtained from:

$$k = \sum_{j=1}^{4}\left(a_j \exp\left[-\left(\frac{\log_{10} f - b_j}{c_j}\right)^2\right]\right) + m_k \log_{10} f + c_k \tag{5}$$

$$\alpha = \sum_{j=1}^{5}\left(a_j \exp\left[-\left(\frac{\log_{10} f - b_j}{c_j}\right)^2\right]\right) + m_k \log_{10} f + c_k, \tag{6}$$

where f is the frequency in GHz. It is important to mention that, as k and α are coefficients that depend on the polarization we will have two different values of k and α, namely, k_H and α_H for horizontal polarization or k_V and α_V for horizontal polarization. In tables 1, 2, 3, and 4 of Recommendation ITU-R P-838-3 [6], the ITU provides the coefficients of k_H, α_H, k_V and α_V.

Furthermore, it is necessary to compute the horizontal reduction factor, $r_{0.01}$, using the following equation:

$$r_{0.01} = \frac{1}{1 + 0.78\sqrt{\frac{d_g \gamma_r}{f}} - 0.38\left(1 - \exp^{-2d_g}\right)}. \tag{7}$$

Additionally, it is essential to calculate the vertical adjustment factor, denoted as $v_{0.01}$, by utilizing the following mathematical formulas:

$$v_{0.01} = \frac{1}{1 + \sqrt{\sin\theta}\left(31\left(1 - \exp^{-\left(\frac{\theta}{(1+X)}\right)}\right)\frac{\sqrt{L_R \gamma_r}}{f^2} - 0.45\right)}, \tag{8}$$

where L_R is a distance that depends on the elevation angle, θ and on $r_{0.01}$ as follows:

$$\zeta = \tan^{-1}\left(\frac{h_r - h_s}{d_g r_{0.01}}\right), \quad \text{(degrees)} \tag{9}$$

when $\zeta > \theta$, then:

$$L_R = \frac{d_g r_{0.01}}{\cos\theta} \quad \text{(km)} \tag{10}$$

else:

$$L_R = d_r \quad \text{(km)} \tag{11}$$

Moreover, in equation *(8)*, X is a constant that is determined by the latitude, denoted as ψ, of the Earth stations. We can derive the value of X as follows: If $|\psi| < 36°$

$$X = 36 - |\psi|, \tag{12}$$

otherwise $X = 0$. In this regard, the effective path length is:

$$L_E = L_R v_{0.01}. \quad \text{(km)} \tag{13}$$

The next step is to compute the predicted attenuation l_p in the effective propagation distance, using the equation provided in [31], as follows:

$$l_p = \gamma_r L_E \quad \text{(dB)} \tag{14}$$

In this context, we use Matlab to compute the equations

we discussed earlier and obtained Fig. 6. This figure displays the rain attenuation in dB per km as a function of frequency, calculated using equation *(4)*. It reveals that the highest attenuation per kilometer is about 30 dB for the City in Brazil, which is a high rain zone. This outcome agrees with Recommendation ITU-R P.618-14 [32].

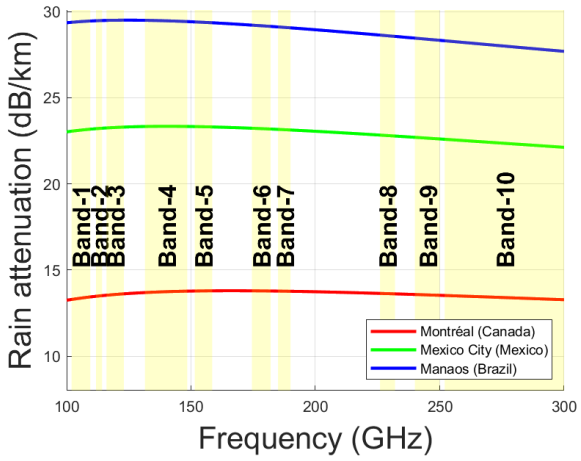

Fig. 6 – Rain attenuation

3.2 Fog and cloud attenuation

According to the ITU [7], fog can have a significant impact on frequencies above 100 GHz. Therefore, in this section, we not only examine the effects of fog but also include the impact of clouds due to their high levels of humidity. The attenuation caused by fog and clouds, denoted as l_{fc}, can be calculated using the method described in Recommendation ITU-R P.840 [7], and the methodology used in [8], as follows:

$$l_{fc} = K_l(f,T)M \quad \text{(dB/km)}, \tag{15}$$

where K_l stands for the cloud liquid water specific attenuation coefficient, f is the frequency in GHz, T is the cloud liquid water temperature in kelvin, and M means the liquid water density in the cloud or fog in g/m^3. K_l could be obtained using the Rayleigh scattering, as follows [7]:

$$K_l(f,T) = \frac{0.819f}{\varepsilon''(1+\eta^2)}, \quad \text{(dB/km)/(g/m}^3\text{)} \tag{16}$$

where:

$$\eta = \frac{2+\varepsilon'}{\varepsilon''}. \tag{17}$$

The complex dielectric permittivity of water could be obtained using the following equations:

$$\varepsilon'' = \frac{f(\varepsilon_0-\varepsilon_1)}{f_p[1+(f/f_p)^2]} + \frac{f(\varepsilon_1-\varepsilon_2)}{f_s[1+(f/f_s)^2]} \tag{18}$$

$$\varepsilon' = \frac{\varepsilon_0-\varepsilon_1}{1+(f/f_p)^2} + \frac{\varepsilon_1-\varepsilon_2}{1+(f/f_s)^2} + \varepsilon_2. \tag{19}$$

Let us denote the principal relaxation frequency as f_p and the secondary relaxation frequency as f_s. These frequencies can be obtained using the following equations:

$$f_p = 20.20 - 146(\Theta-1) + 316(\Theta-1)^2 \quad \text{(GHz)} \tag{20}$$

$$f_s = 39.8 f_p \quad \text{(GHz)} \tag{21}$$

Regarding ε_0, ε_1 and ε_2, these are permittivity constants. ε_0 and ε_1 can be computed using equations from *(22)* to *(23)*, ε_2 is equal to 3.52, and

$$\varepsilon_0 = 77.66 + 103.3(\Theta-1) \tag{22}$$

$$\varepsilon_1 = 0.0671\varepsilon_0. \tag{23}$$

For equation *(22)*, Θ is the relative inverse temperature and can be computed as $\Theta = 300/T$, where T is the liquid water temperature in kelvin.
Additionally, the attenuation due to fog and cloud l_{cf} could be computed using the following equation:

$$l_{cfdB} = \frac{L(p)K_l(f,T)}{\sin\theta}, \quad \text{(dB)} \tag{24}$$

where θ is the elevation angle, and $L(p)$ is the reduced total columnar content of liquid water which is in Kg/m^2. It could be obtained from the maps published by ITU as part of Recommendation P.840-8 [7]. For a probability which exceeds 0.015% of the year, the values of $L(p)$ are 1.33344811, 1.33344811 and 0.79152631247476 Kg/m^2 for Montreal, Mexico City and Manaos, respectively,
As we mentioned before, for this case, the existing model to compute the attenuation is valid for frequencies below 200 GHz; however, in [17], [8] and [33], it is mentioned that above this limit, the use of Mie theory is necessary to evaluate both scattering and absorption contributions of liquid water droplets. This model is used to calculate the attenuation based on the measured distribution of droplet sizes. Thus, the fog and cloud fading can be obtained using the following equation:

$$l_{fc} = 4.343 \cdot 10^3 \int_0^\infty Q(r)n(r)dr, \quad \text{(dB/km)} \tag{25}$$

where $Q(r)$ is the extinction cross-section[1] of fog droplet, which can be computed using equation *(26)*, and $n(r)$ is the drop size distribution. In equation *(26)*, a_n and b_n are the Lorenz–Mie coefficients

$$Q(r) = \frac{\lambda^2}{2\pi}\sum_{n=0}^{\infty}(2n+1)\Re(|a_n|^2+|b_n|^2). \tag{26}$$

In this context, we use the Matlab tool to compute the equations we discussed earlier and obtained Fig. 7. This figure displays the fog and cloud attenuation in dB per km as a function of frequency (ranging from 100 GHz to

[1] *"The area that, when multiplied by the irradiance of electromagnetic waves incident on an object, gives the total radiant flux scattered and absorbed by the object."[34]*

300 GHz), calculated using equations *(15)* and *(25)*. The figure reveals that the highest attenuation per kilometre is about 8 dB for the City in Brazil. This outcome agrees with Recommendation ITU-R P.840 [7].

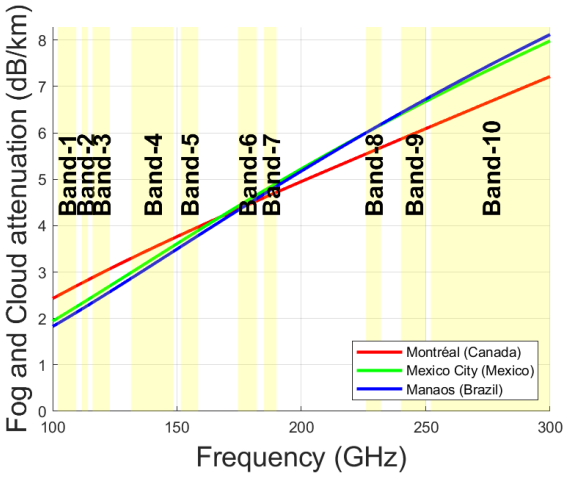

Fig. 7 – Fog and cloud attenuation

3.3 Atmospheric gas attenuation

The atmospheric gas attenuation l_g could be obtained from [9]:

$$l_g = \gamma_o + \gamma_w = 0.1820 f(N_o(f) + N_w(f)) \quad \text{(dB/km)} \tag{27}$$

where γ_o and γ_w are the specific attenuations due to dry air and water vapour, respectively, f is the frequency in GHz, and $N_o(f)$ and $N_w(f)$ are the imaginary parts of the frequency-dependent complex refractivities:

$$N_o(f) = \sum_i S_i F_i + N_D(f) \tag{28}$$

$$N_w(f) = \sum_i S_i F_i, \tag{29}$$

where S_i is the strength of the ith oxygen or water vapour line that can be obtained from: For exigent:

$$S_i = (a_1 \times 10^{-7})\Theta^3 \exp[a_2(1-\theta)](p), \tag{30}$$

and for water vapour:

$$S_i = (b_1 \times 10^{-1})\Theta^{3.5} \exp[b_2(1-\theta)](w), \tag{31}$$

where $\Theta = 300/T$, T is the temperature in kelvin. p is the dry air pressure in hPa, and w is the water vapour partial pressure in hPa. The vapour pressure w can be computed depending of the water-vapour density ρ ,using the following equation:

$$w = \frac{\rho T}{216.7}. \tag{32}$$

Furthermore, $N_D(f)$ is the dry continuum, which arises a pressure-inducted nitrogen attenuation above 100 GHz. $N_D(f)$ can be obtained from:

$$N_D(f) = fp\Theta^2 \left[\frac{6.14 \times 10^{-5}}{d_e \left[1 + \left(\frac{f}{d_e}\right)^2\right]} + \frac{1.4 \times 10^{-12} p\Theta^{1.5}}{1 + 1.9 \times^{-5} f^{1.5}} \right], \tag{33}$$

where d_e is the Debye spectrum: $d_e = 5.6 \times 10^{-4}(p + w)\Theta^{0.8}$. On the other hand, F_i is the oxygen or water vapour line shape factor, and the summations extend over all the spectral lines indicated in tables 1 and 2 of Recommendation ITU-R P.676-13 [9]:

$$F_i = \frac{f}{f_i}\left[\frac{\Delta f - \delta(f_i - f)}{(f_i - f)^2 + \Delta f^2} + \frac{\Delta f - \delta(f_i + f)}{(f_i + f)^2 + \Delta f^2}\right], \tag{34}$$

where f_i stands for the oxygen or water vapour line frequency and Δf is the width of the line [9]:

For oxygen it becomes

$$\Delta f = a_3 \times 10^{-4}(p\Theta^{(0.8-a_4)} + 1.1w\Theta), \tag{35}$$

and for water vapour:

$$\Delta f = b_3 \times 10^{-4}(p\Theta^{b_4} + b_5 w\Theta^{b_6}) \tag{36}$$

In the second part, it is necessary to obtain the slant path of the gaseous attenuation for the communication from Earth to space or vice versa (including near-to-Earth communications, for example, aeronautical ESIMs). For this, in [9], the ITU proposes dividing the signal path into different layers, as shown in Fig. 8. The thickness δ_i of each layer could be obtained from the following equation:

$$\delta_i = 0.0001 e^{\frac{i-1}{100}}, \quad \text{(km)} \tag{37}$$

Additionally, a_1, a_2, and a_3 are the path lengths that the signal goes through each layer; they can be calculated from equations *(38)* [9]. Layers have a different radio refractive index η_i, whose values could be calculated from [35]. Furthermore, α_i and β_i are the entry and exit incidence angles in each layer; they can be calculated from equations *(39)*, *(40)* and *(41)*. r_i is the radius from the

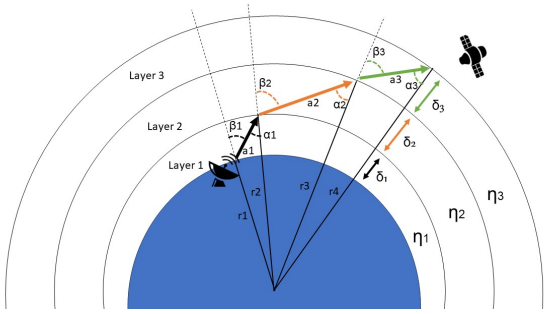

Fig. 8 – Slant path gaseous attenuation for the communication Earth to space

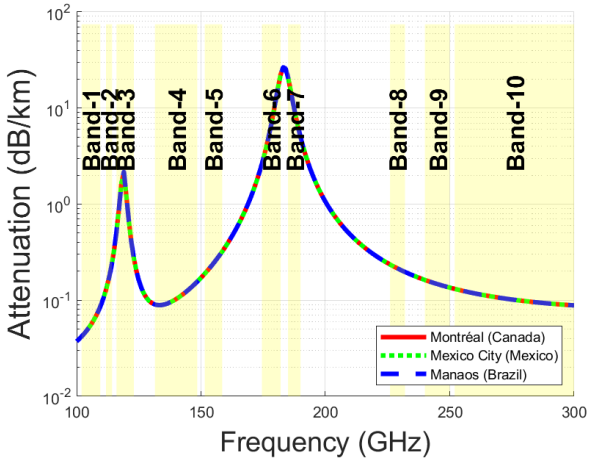

Fig. 9 – Atmospheric gases attenuation in dB/km

center of the Earth to the beginning of each layer.

$$a_i = -r_i \cos\beta_i + \sqrt{r_i^2 \cos^2\beta_i + 2r_i\delta_i + \delta_i^2} \quad \text{(km)} \quad (38)$$

$$\alpha_i = \sin^{-1}\left(\frac{r_i}{r_i + \delta_i}\sin\beta_i\right) \quad (39)$$

$$\beta_1 = 90 - \theta, \quad (40)$$

where θ is the elevation angle of the Earth station. And for $i > 1$ we can compute β using the following equation:

$$\beta_i = \sin^{-1}\left(\frac{n_1 r_1}{n_i r_i}\sin\beta_1\right), \quad (41)$$

where n_i is a function of the temperature, pressure and the vapour pressure mentioned in equation *(32)*, that can be computed using equation *(42)* proposed in [35].

$$n = 1 + \left[77.6\frac{P_d}{T} + 72\frac{w}{T} + 3.75\times10^5\frac{w}{T^2}\right](1\times10^{-6}). \quad (42)$$

To calculate the specific attenuation in dB, we can apply the results from equations *(27)* and *(38)* to derive the following equation:

$$A_{gas} = \sum_{i=1}^{i_{max}} a_i l_{g_i} \quad \text{(dB)}. \quad (43)$$

Furthermore, it is valid to compute the attenuation in dB in a simpler form with the following equation:

$$A_{gas} = \frac{l_g}{\sin\theta} \quad \text{(dB)} \quad (44)$$

In this context, Fig. 9 illustrates the atmospheric gases attenuation in dB/km as a function of frequency and elevation angle, computed from equation *(27)*. The results are consistent with Recommendation ITU-R P.676-13 [9].

3.4 Free space attenuation

The free space attenuation l_f could be obtained from [20]:

$$l_f = 20\log_{10}\left(\frac{4\pi d}{\lambda}\right), \quad \text{(dB)} \quad (45)$$

where, d is the distance from the transmitter to the receiver.

Additionally, according to the attitudes and links mentioned in Subsection 2.1 and the parameters mentioned in Table 3, the slant range d described in [36] was obtained using the following equation:

$$d_s = R_E\left[\sqrt{\left(\frac{h + R_E}{R_E}\right)^2 - \cos^2\theta} - \sin\theta\right]. \quad \text{(km)} \quad (46)$$

In this context, the values of free-space attenuation for the specific frequencies between 100 - 300 GHz are shown in figures 10, 11 and 12. It is important to note that the results shown in Fig. 10 are only applicable to Earth-station to satellite links or vice versa, and for the aeronautical ESIMs. The results for inter-satellite links are shown in figures 11 and 12.

These figures show a clear trend of increasing attenuation with increasing altitude and frequency, with the highest attenuation value being around 220 dB. This means that the signal strength decreases as it travels through free space, especially at higher altitudes and frequencies.

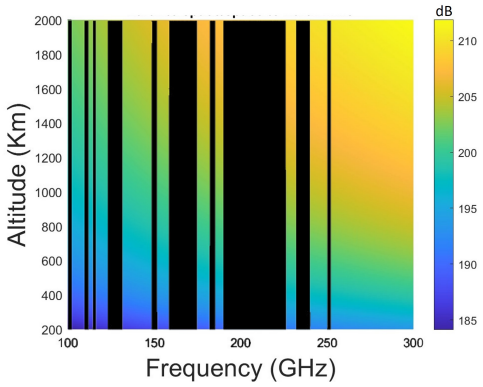

Fig. 10 – Free space attenuation Earth station to satellite

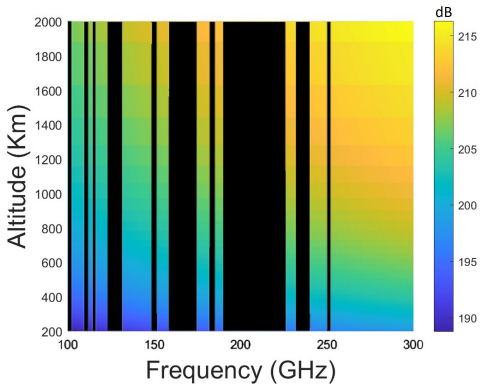

Fig. 11 – ISL between satellites in the same orbit

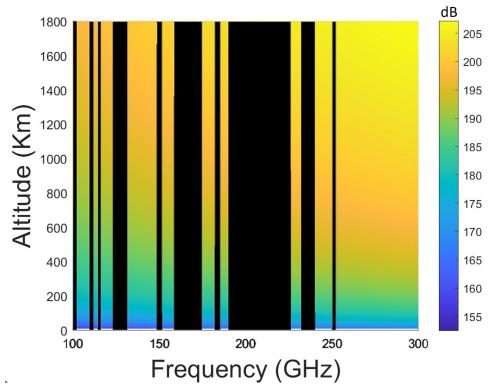

Fig. 12 – ISL between satellites in different orbits

Furthermore, to standardize the link-budget calculation, we use the free attenuation in dB/km as a reference value. This value is obtained by dividing the previous results or subtracting in dB, by the distance of each link. The results are shown in Fig. 13.

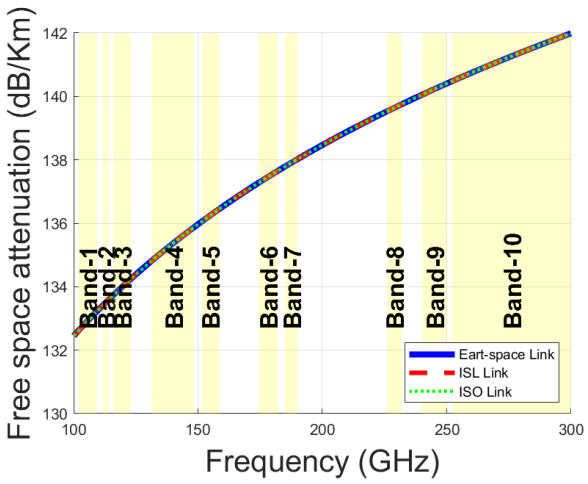

Fig. 13 – Free-space attenuation

4. NUMERICAL RESULTS

4.1 Total attenuation

The total loss was obtained by adding the respective values of rain, fog, cloud, atmospheric gases, and free space. The results are shown in figures 14 and 15.

Fig. 14 illustrates the impacts for both Earth station to satellite and satellite to Earth station links. These findings are also relevant for the links between the A-ESIM and the satellites since the altitude difference between an Earth station on land and one on board an aircraft is negligible (around tens of kilometers) in comparison to the distance of LEO satellites, which are hundreds or thousands of kilometers away.

From Fig. 14, it is possible to see that the total attenuation generally increases with frequency, with a peak of around 180 GHz due to the ionospheric gases attenuation. This peak of more than 195 dB/km impacts Band-6 and Band-7. Fig. 15 illustrates the impact on ISL, where free-space

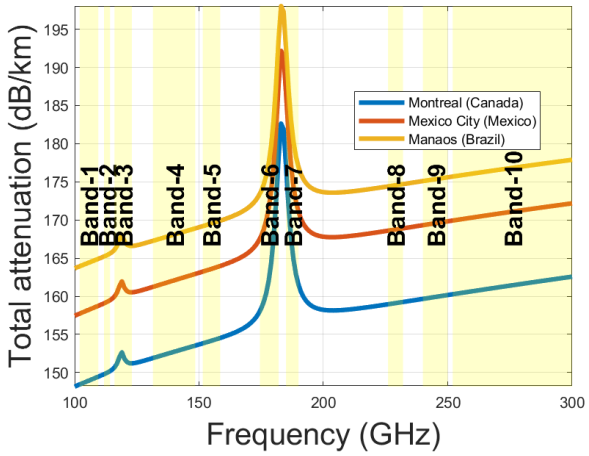

Fig. 14 – Total attenuation - Earth station to satellite link and satellite to Earth station link

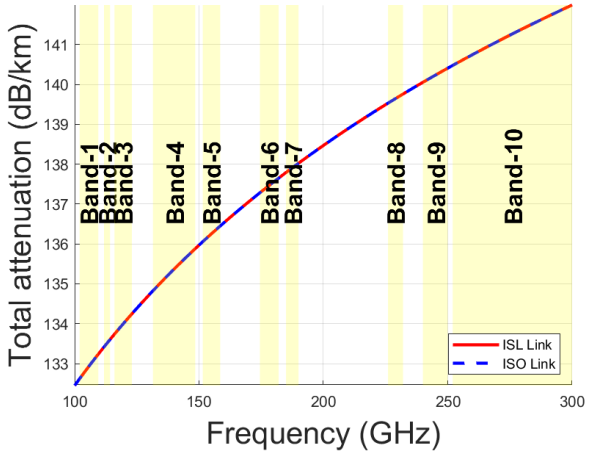

Fig. 15 – Total attenuation- ISL and inter-satellite orbit links

loss is the main factor that affects them, even in satellites in the same orbit or in different orbits. These links operate at high altitudes where the atmosphere has minimal impact. Hence, we neglect the effects of rain, fog, clouds or atmospheric gases on these links. The highest attenuation is observed at 300 GHz, with a peak of 141.99 dB/km (Band-10), while the lowest attenuation is observed at 102 GHz, with a trough of 132.44 dB/km.

4.2 Link budget

In this subsection, we calculate the link budget for uplink, downlink and inter-satellite links. A link budget is a calculation of the total losses and gains from the transmitter to the receiver in a wireless communication system, including the transmitted power [37].

For computing the power received P_{rx} at the Earth station antenna or at the satellite antenna, we use the following equation:

$$P_{rx} = P_{tx} + G_{tx} + G_{rx} - h_l, \quad \text{(dB)} \qquad (47)$$

where P_{tx} is the transmitted power, G_{rx} is the gain in

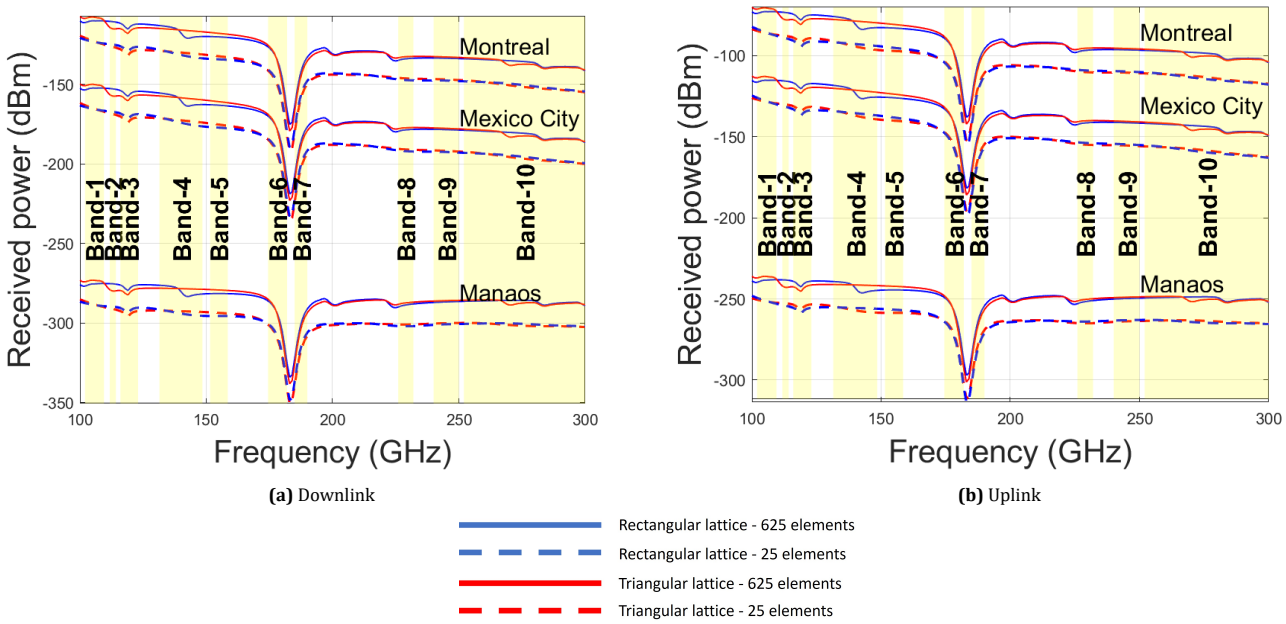

(a) Downlink

(b) Uplink

Fig. 16 – Received power per link

reception, and G_{tx} is the gain in transmission. In this regard, the values of P_{tx} for satellites and the Earth station, and G_{rx} of the Earth station that we took into account for our computations are indicated in Table 3. Additionally, we considered the total attenuation, h_l, analyzed in the past subsection. For the satellite's antenna gain, we consider the values computed for the uniform rectangular phased array, that are shown in figures 3 and 4.

4.2.1 Downlink and uplink

The results of the transmitted power are shown in figures 16a and 16b, where the lines in blue correspond to computations for the rectangular lattice, while red lines correspond to the triangular lattice. Furthermore, the dotted lines denote an array of 25 elements (worst case scenario), and the solid lines are for antennas with 625 elements (best case scenario). Figures 16a and 16b reveal that bands 6 and 7 register the lowest received power, principally attributable to a pronounced peak of attenuation within these bands due to the atmospheric gases. Moreover, Manaos records the minimum power values at the Earth station. To facilitate effective communication in Manaos, the use of low noise amplifiers with an extensive operational range should be considered. This strategy would bolster our capacity to recover signals transmitted by the LEO satellites. Moreover, the data indicates a trend of decreasing received power as frequency increases across three cities. Specifically, at the Earth station, the power values range from -191.5951 dBm to -107.2536 dBm in Montreal, -235.3337 dBm to -149.6186 dBm in Mexico City, and -350.6654 dBm to -273.057 dBm in Manaos. For the satellite antenna, from Fig. 16b we can see that the received power ranges from -70.2536 dBm to -154.5951 dBm in Montreal, -112.6186 dBm to -198.3337 dBm in Mexico City, and -236.057 dBm to -313.6654 dBm in Manaos.

When comparing the architectures of the phased array, it is apparent that there is not a significant difference in the power received between the two. However, the factor that distinguishes them is the number of elements incorporated into the phased array. The design with 625 elements yields the best performance.

It is worth noting that the transmitted power by the satellite that we consider is 29 dBW, a standard value for satellites in contemporary LEO maga-constellations such as Starlink. However, our findings indicate that this power level is insufficient, as our signal is significantly affected by propagation attenuation due to the high frequencies. To address this, we increased the received power in the downlink to the following values: 33.01 dBW, 37 dBW, 40 dBW, and 100 dBW. The outcomes of these adjustments are illustrated in figures 17, 18 and 19, where the dotted lines denote a phase array with the triangular lattice and, the solid lines signify an phase array with the rectangular lattice.

As discerned from the referenced figures, there exists a direct relationship between the escalation in transmitted power by the satellite and the enhancement in received power at the Earth station. The ideal scenario is realized with a transmission power of 100 dBW, yielding a received power of -36.6 dBm for Montreal, -79.34 dBm for Mexico City and -202.2 dBm for Manaos. However, achieving a transmission power of 100 dBW for a LEO satellite could be challenging. A more attainable maximum value for the transmitting power might be 40 dBW. With this power, it is possible to achieve received power

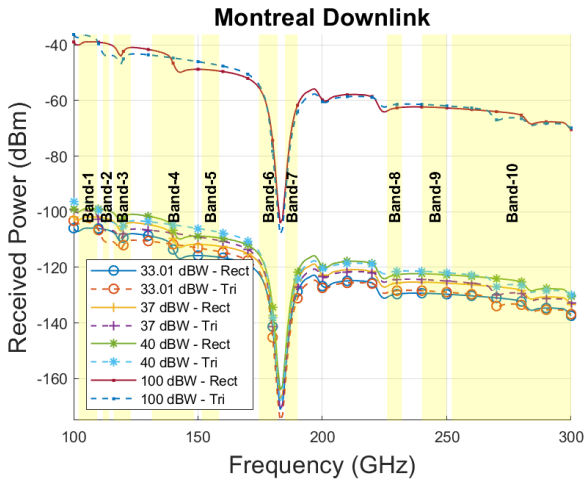

Fig. 17 – Received power in Montreal for different values of P_{tx}

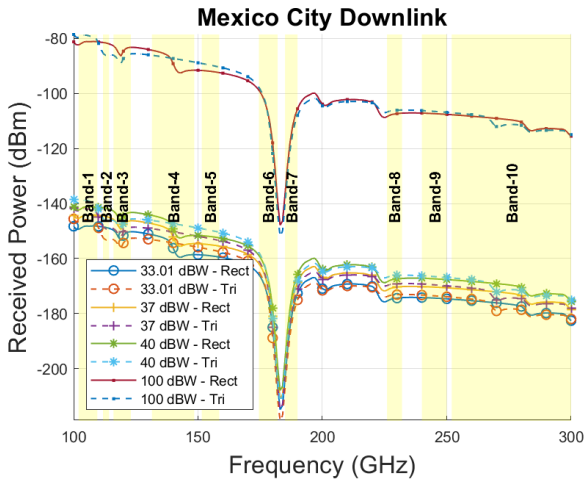

Fig. 18 – Received power in Mexico City for different values of P_{tx}

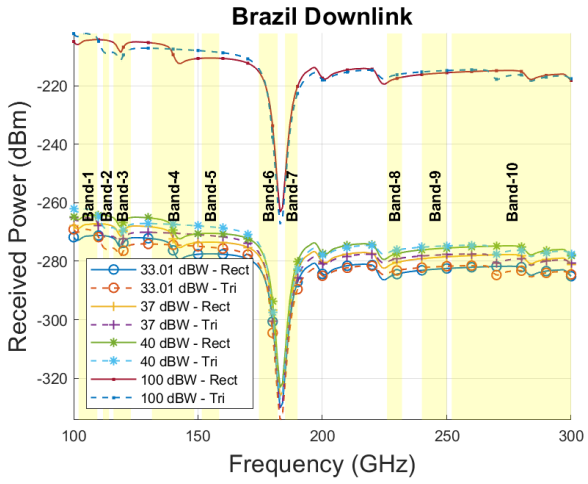

Fig. 19 – Received power in Manaos for different values of P_{tx}

values around -96.76 dBm and -130 dBm for Montreal, -140 dBm and -174.986 dBm for Mexico City, and -262.1 dBm and -277.152 dBm for Manaos.

It is important to mention that the aforementioned analysis takes into account weather conditions such as rain, fog, clouds and atmospheric gases, all occurring simultaneously. In this context, our results represent a critical scenario. However, under clear, blue sky conditions, we can achieve improved results.

Therefore, we also computed the link budget for downlink and uplink, considering only the free-space loss that is shown in Fig. 15, and a transmitted power of 29 dBW. The results are depicted in Fig. 20. The blue lines correspond to the results for rectangular phase arrays with 625 elements, while the red lines represent rectangular phase arrays with 25 elements. The green lines are associated with triangular phase arrays comprising 625 elements, and the black lines denote triangular phase arrays with 25 elements. Furthermore, solid lines consider the minimum free space attenuation observed at satellites at an altitude of 200 km, while dashed lines consider the maximum free space attenuation observed at satellites at an altitude of 2000 km. It is important to mention that these results are applicable to the three cities under study.

From Fig. 20 we can observe that the received power is similar between the different architectures of the antennas. The best scenario is observed for the communications with satellites that operates at an altitude of 200 km, yielding a maximum received power of 17.59 dBm using a phase array that has 625 elements. For satellites in an altitude of 2000 km it is possible to reach up to -46 dBm.

Upon comparing figures 16 and 20, it becomes evident that weather conditions play a crucial role in determining the minimum received power achievable in both downlink and uplink scenarios. This is particularly significant for the downlink due to the power transmission limitations of a LEO satellite.

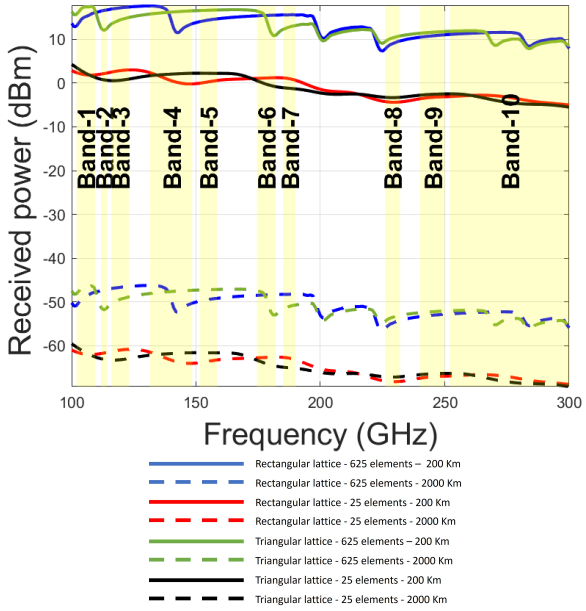

Fig. 20 – Received power for downlink considering blue sky conditions

4.2.2 *Inter-satellite links*

Regarding the received power for inter-satellite communications within the same orbit, the results are shown in Fig. 21. The upper sub-figure presents data related to the rectangular lattice, while the lower sub-figure illustrates the triangular lattice. In the figure, the blue lines denote computations for an array comprising 625 elements, and the red lines correspond to an array with 25 elements. We employ solid lines to represent the received power in satellites at an altitude of 200 km. Dashed lines are used to signify satellites at an altitude of 1000 km, and dash-dotted lines indicate satellites at an altitude of 2000 km.

Upon scrutinizing Fig. 21, we observe that the received power exhibits a pattern of horizontal peaks and valleys, each appearing within specific bands. This pattern is more conspicuous for the phase arrays comprising 625 elements, whereas the antennas with 25 elements display less significant variations. Nevertheless, the phase arrays with 625 elements demonstrate superior performance compared to those with 25 elements. Furthermore, we discerned that both lattices work in synergy to maintain a consistent power level. For instance, in Band-4, while the rectangular lattice shows a dip in the middle of the band, the triangular lattice ascends to a peak.

Interestingly, both architectures demonstrate identical received power values but in different frequencies. The maximum received power, p_{rx}, is -72.7954 dBm, observed in communications between satellites in the 200 km-orbit equipped with a phase array of 625 elements. In contrast, the minimum values, ranging approximately between -130.357 dBm and -102.466 dBm, are associated with antennas comprising 25 radiating elements.

On the other hand, results about the power received in communications between satellites in different orbits are

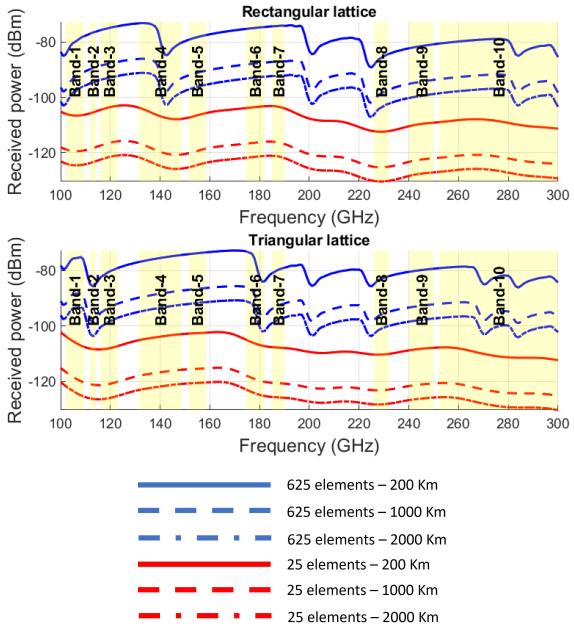

Fig. 21 – ISL received power for frequencies between 100 - 300 GHz

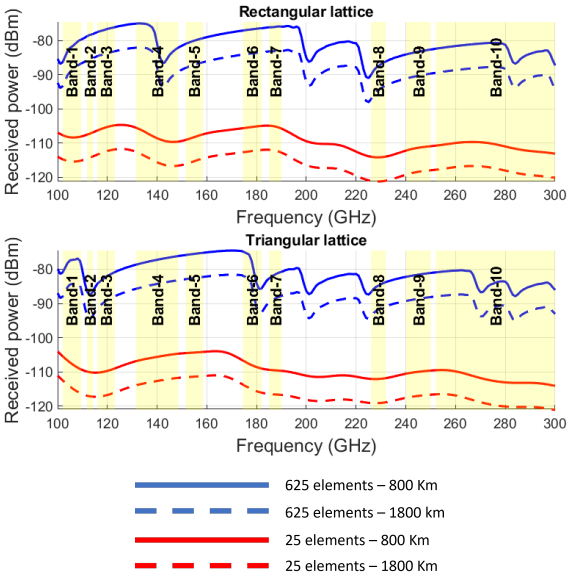

Fig. 22 – ISO received power for frequencies between 100 - 300 GHz

depicted in Fig. 22. The upper sub-figure contains information for the rectangular lattice, while the lower sub-figure presents data for the triangular lattice. In the figure the blue lines represent computations for an array consisting of 625 elements, while the red lines correspond to an array with 25 elements. Solid lines are used to indicate the received power in satellites at an altitude of 200 km, communicating with other satellites at an altitude of 1000 km (800 km of distance. Dashed lines depict satellites at an altitude of 200 km communicating with other satellites at an altitude of 2000 km (1800 km of distance. From Fig. 22, we note that the received power in inter-orbit communications exhibits a behaviour similar to that in same-orbit communications. It displays a pattern of horizontal peaks and troughs, each occurring within distinct bands. This pattern is more evident for the phase arrays with 625 elements, while the antennas with 25 elements show less pronounced variations. However, the phase arrays with 625 elements demonstrate superior performance compared to those with 25 elements. Furthermore, both architectures exhibit comparable received power values. The maximum received power is -74.7093 dBm, observed in the communications between satellites with a distance of 800 km equipped with a phase array of 625 elements. In contrast, the minimum values, which range approximately between -121.187 dBm and -104.881 dBm, correspond to antennas comprising 25 radiating elements.

4.3 Signal-to-noise ratio

To obtain the Signal-to-Noise-Ratio (SNR or Carrier-to-Noise ratio (C/N in dB, we can use equation *(48)* [36], where T_s is the noise temperature of the system, B is the bandwidth, the relation of $P_{tx} + G_{tx} - h_l + G_{rx}$ is the received power that we analysed in the last subsection, and as we mentioned before, h_l is the total attenuation.

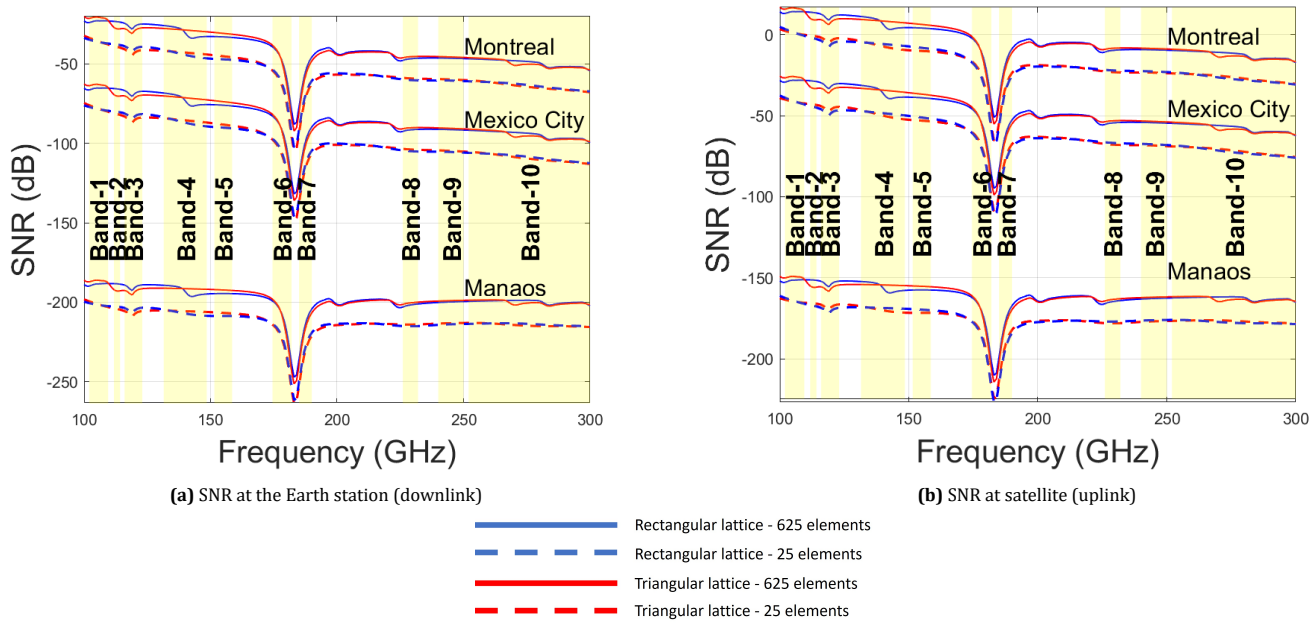

(a) SNR at the Earth station (downlink)

(b) SNR at satellite (uplink)

Fig. 23 – SNR per link

According to [36], a reasonable value for the noise temperature is $T_s = 290K$. Thus, we took into consideration the value for our computations. Additionally, we considered bandwidth of 500 MHz, using the SNR formula below.

$$\frac{S}{N_0} = P_{tx} + G_{tx} - h_l + G_{rx} - 10 * \log_{10}(T_s \times B) + 228.6 \quad (48)$$

4.3.1 *Downlink and uplink*

Regarding the communication between Earth stations and satellites, figures 23a and 23b show the SNR that we got at the Earth station and at the satellite antenna. The lines in blue correspond to computations for the rectangular lattice, while red lines correspond to the triangular lattice. Furthermore, the dotted lines denote an array of 25 elements, and the solid lines are for the array with 625 elements.

From the figures the data indicates a trend of decreasing SNR as frequency increases; this is due to having more attenuation at higher frequencies. Additionally, when comparing the architectures of the phased array, it becomes clear that there is not a substantial difference in the SNR between the two. However, the number of elements incorporated into the phased array serves as the distinguishing factor. Notably, the design incorporating 625 elements exhibits the most effective performance.

Moreover, we observed that Band-6 and Band-7 have the weakest SNR for both links across the three cities. This is due to a significant peak of attenuation in these bands, due to the atmospheric gases. In terms of the SNR performance among the cities, Manaos records the minimum values at the Earth station, while Montreal demonstrates the best performance.

Specifically, for the satellite antenna, according to Fig. 23b the SNR ranges from 16.7317 dB to -67.6097 dB in Montreal, -25.6331 dB to -111.3482 dB in Mexico City and -149.0715 dB to -226.6799 dB in Manaos. From these results, we can observe that we reached a maximum SNR of 16.7317 dB for Band-1 to Band-5. However, for the other bands, we turn back to negative values for the SNR, which means that the noise is much higher than the transmitted signal. In this case, we would increase the power transmitted by the Earth station in order to raise the SNR.

At the Earth station, the SNR values range from -20.2682 dB to -104.6097 dB in Montreal, -62.6331 dB to -148.3482 dB in Mexico City, and -186.0715 dB to -263.6799 dB in Manaos. From these results, we can observe that we have a considerable SNR for the downlink; this is especially impacted by the attenuation, and due to this the transmitted power cannot be increased, usually no more than 800 W (29 dBW).

As we mentioned before, in order to improve the performance of the downlink, we increase the values of transmitted power by the satellites to the following values: 33.01 dBW, 37 dBW, 40 dBW and 100 dBW. The results of these adjustments are shown in figures 24, 25, and 26, where the dotted lines denote a phase array with the triangular lattice and the solid lines signify a phase array with the rectangular lattice.

The figures previously mentioned illustrate a clear relationship between the augmentation of transmitted power and the enhancement in the SNR. The most favourable condition is obtained with a transmission power of 100 dBW, which yields an SNR of 44.4 dB for Montreal, 1.89 dB for Mexico City and -121.25 dB for Manaos. From

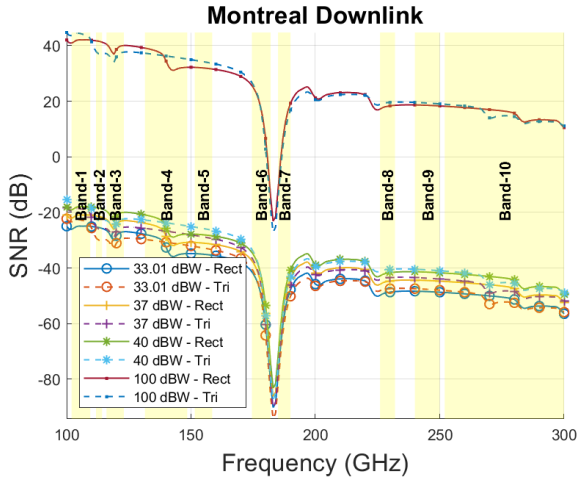

Fig. 24 – SNR at the Earth station in Montreal for different values of P_{tx}

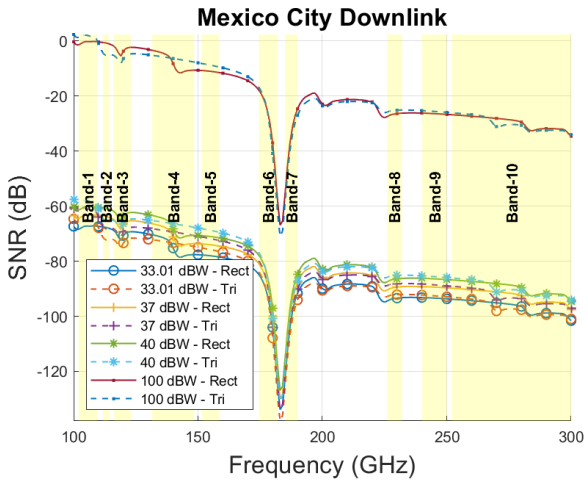

Fig. 25 – SNR at the Earth station in Mexico City for different values of P_{tx}

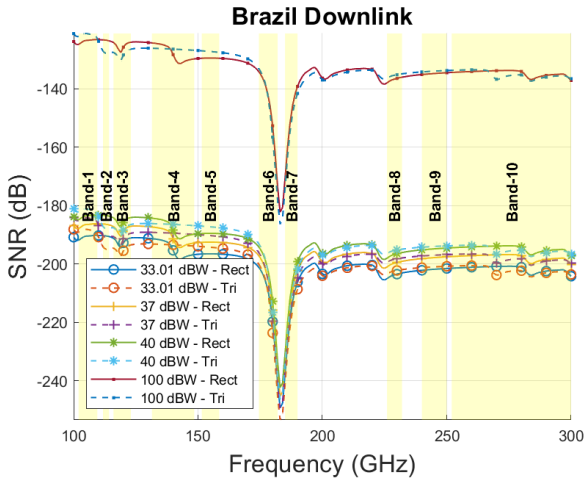

Fig. 26 – SNR at the Earth station in Manaos for different values of P_{tx}

this exercise, we can infer that the SNR escalates with an increase in transmitted power. However, for LEO satellites, which attain 100 dBW with the current technology presents a challenge. It is crucial to note that the aforementioned analysis represents a critical scenario. Under ideal conditions, such as clear, blue sky weather, we can anticipate improved results.

In this regard, we also computed the SNR for downlink and uplink, considering only the free-space loss (see Fig. 13), a transmitted power of 29 dBW and a bandwidth of 500 MHz. The results are depicted in Fig. 27, where the blue lines correspond to the results for rectangular phase arrays with 625 elements, while the red lines represent rectangular phase arrays with 25 elements. The green lines are associated with triangular phase arrays comprising 625 elements, and the black lines denote triangular phase arrays with 25 elements. Furthermore, solid lines consider the minimum free space attenuation observed at satellites at an altitude of 200 km, while dashed lines consider the maximum free space attenuation observed at satellites at an altitude of 2000 km. It is important to mention that these results are applicable to the three cities under study.

From Fig. 27 we can observe that the SNR is similar between the different architectures of the antennas. The best scenario is observed for the communications with satellites that operate at an altitude of 200 km, yielding a maximum SNR of 104.4 dB using a rectangular or triangular phase array that has 625 elements. For satellites in an altitude of 2000 km, it is possible to reach up to 40.7 dB.

Upon comparing figures 23 and 27, it becomes evident that weather conditions play a crucial role in determining SNR achievable in both downlink and uplink scenarios. This is particularly significant for the downlink due to the power transmission limitations of a LEO satellite. Furthermore, our analysis suggests that for a satellite system operating in the 100 to 300 GHz frequency range, it is essential to allocate frequencies based on prevailing

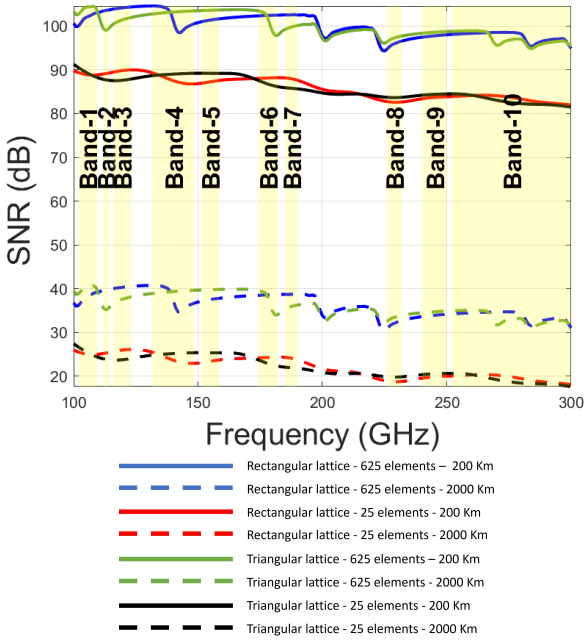

Fig. 27 – SNR for downlink considering blue sky

weather conditions.

4.3.2 Inter-satellite links

Regarding the SNR for communication between satellites in the same orbit, the results are shown in Fig. 28, where the superior sub-figure considers the information for the rectangular lattice and in the inferior sub-figure the triangular lattice. Furthermore, in the figure the lines in blue correspond to computations considering an array of 625 elements, and the red lines are for the array with 25 elements. Additionally, we use solid lines to denote the SNR in satellites at an altitude of 200 km, dashed lines represent satellites at an altitude of 1000 km, and dash-dotted lines indicate satellites at an altitude of 2000 km.

From Fig. 28 we can observe that the SNR follows a trend of horizontal peaks and troughs, each manifesting within distinct bands. This trend is more pronounced for the phase arrays with 625 elements, while the antennas with 25 elements exhibit less pronounced fluctuations. However, the phase arrays with 625 elements outperform those with 25 elements.

Additionally, both architectures demonstrate similar SNR values. The SNR in ISL will range between 13.73 dB and -43.3824 dB. The maximum value was observed in the communication between satellites in the 200 km-orbit equipped with a phase array of 625 elements and the minimum values are associated with antennas comprising 25 radiating elements.

Mostly, we have positive values for the ISL SNR in all the bands under study for both types of lattice, considering 625 radiating elements. However, when we consider a minimum of 25 of radiating elements, we turn back to negative values for the SNR, ranging from -20 to -40 dB.

On the other hand, results about the SNR for the communication between satellites in different orbits are depicted in Fig. 29, where, as we mentioned before, the lines in blue correspond to the computations considering an array of 625 elements, and the red lines are for the array with 25 elements. Solid lines are used to indicate the SNR in satellites at an altitude of 200 km, communicating with other satellites at an altitude of 1000 km (800 km of distance). Dashed lines depict satellites at an altitude of 200 km communicating with other satellites at an altitude of 2000 km (1800 km of distance).

From Fig. 29 we can observe that the antenna with the rectangular lattice has a similar SNR performance in comparison with the triangular lattice. Additionally, we note that the SNR in inter-orbit communications exhibits a behaviour similar to that in same-orbit communications, namely, it displays a pattern of horizontal peaks and troughs, each occurring within distinct bands. This pattern is more evident for the phase arrays with 625 elements, while the antennas with 25 elements show less pronounced variations. However, the phase arrays with 625 elements demonstrate superior performance compared to those with 25 elements.

In general, for both types of antenna, the SNR in Inter Satellite Orbit (ISO) links ranges between 10.1075 dB and -34.2120 dB. From these results, we can observe that we reached a maximum SNR of 10.1075 dB for Band-2,Band-3, Band-4, Band-6 and Band-7, with the rectangular lattice. However, for the other bands, we turn back to negative values for the SNR. For the triangular lattice antenna, all of the SNR values range between -5 to -20 dB.

It is important to mention that due to the changes in the elevation angle in antennas of non-geostationary satellites, the signal-to-noise spectral density ratio varies. This is principally thanks to the elevation impacts the attenuation that affects the signal [36].

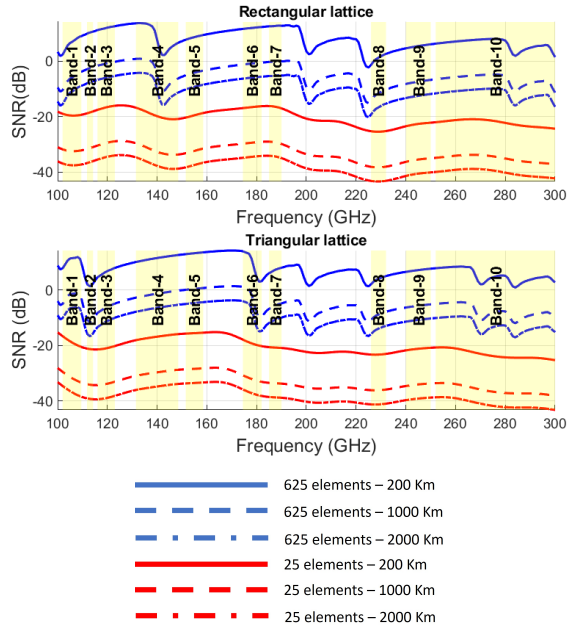

Fig. 28 – ISL SNR for frequencies between 100 - 300 GHz

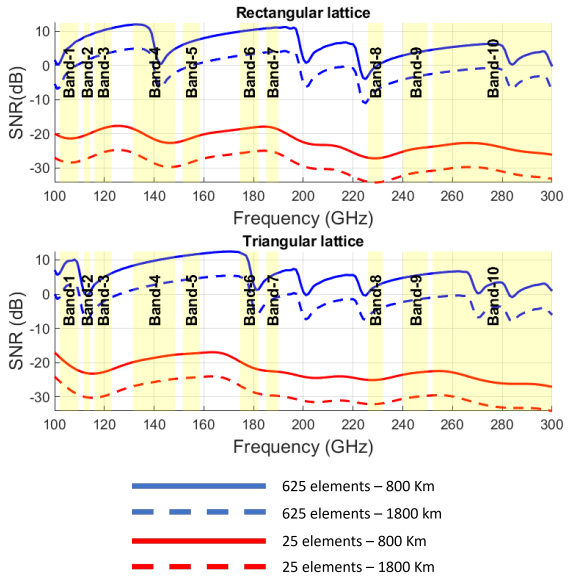

Fig. 29 – ISO SNR for frequencies between 100 - 300 GHz

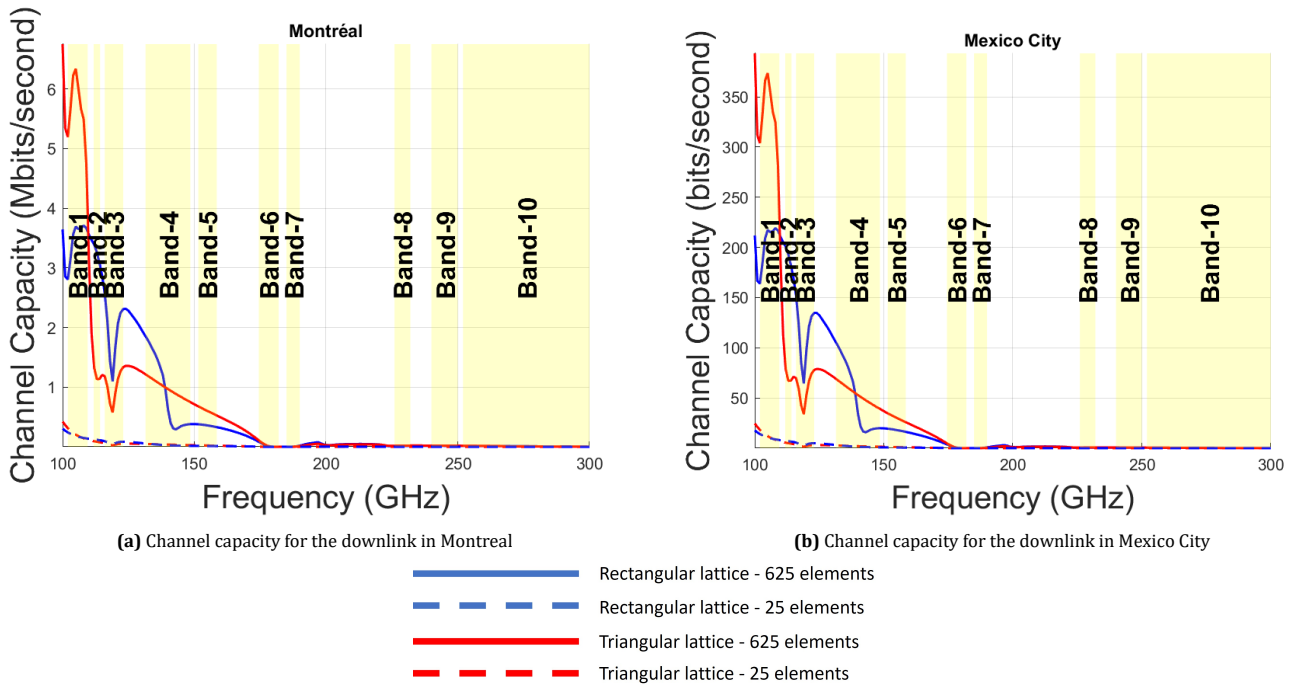

(a) Channel capacity for the downlink in Montreal

(b) Channel capacity for the downlink in Mexico City

Fig. 30 – Channel capacity for frequencies between 100 - 300 GHz (500 MHz bandwidth)

4.4 Channel capacity

The channel capacity is the speed at which data can be sent over a certain communication channel [38]. It is influenced by the channel's bandwidth (how much data it can handle at once) and the SNR (how clear the signal is). The data rate can also change based on the system's modulation scheme (how the data is changed for transmission), coding rate (how much data is sent at once), and bandwidth efficiency (how well the bandwidth is used)[38].

The channel capacity can be calculated using equation *(49)* as referenced in [39]. This equation allows us to determine the maximum achievable spectral efficiency of the Additive White Gaussian Noise (AWGN) channel as a function of the SNR [39]. For equation *(49)*, we considered a bandwidth of 500 MHz, and the capacity is calculated as follows:

$$C = B\log_2(1 + SNR). \quad \text{(bits/s)} \qquad (49)$$

4.4.1 Downlink and uplink

Regarding the communication between Earth stations and satellites, the results are depicted in figures 30 and 31. The blue lines represent computations for the rectangular lattice, while red lines correspond to the triangular lattice. Furthermore, the dotted lines denote an array consisting of 25 elements, while the solid lines correspond to an array with 625 elements.

In Fig. 30, we illustrate the channel capacity for the downlink across Montreal and Mexico City. Meanwhile, Fig. 31 depicts the uplink data for these cities. It is noteworthy that the data for Manaos is excluded due to its negligible values, attributable to the city's low SNR.

Figures 30 and 31 indicate that bands from 6 to 10 have the weakest channel capacity for both cities, due to the low values of SNR in those bands. Mexico City records the lowest data rate values for both links. However, the downlink has the worst performance for both cities.

Regarding the maximum values of data rate achievable, bands 1 and 2 demonstrate the highest channel capacity. Specifically, Montreal reaches up to 7 Mbits/s for the downlink and up to 2.8 Gbits/s for the uplink. While in Mexico City up to 375 bits/s for the downlink and around 1.8 Mbits/s for the uplink, in the same bands.

In contrast, the channel capacity for the remaining bands is approximately zero. These results are an effect of the high attenuation that we have beyond 170 GHz.

The difference between the downlink and the uplink channel capacity is due to the difference in transmitted power by satellites and Earth stations. Earth stations have more capacity to transmit high power than satellites. They usually are limited to 800 W.

When comparing the architectures of the phased array, it is apparent that the rectangular lattice has a better performance that the triangular lattice. Additionally, the factor that distinguishes them is the number of elements incorporated into the phased array. The design with 625 elements yields the best performance.

It is important to note that the data rates values mentioned previously are considerably low. In this regard, we recalculated the channel capacity for both the uplink and downlink, this time taking into account a bandwidth of 5 GHz. The results are illustrated in Fig. 32. As previ-

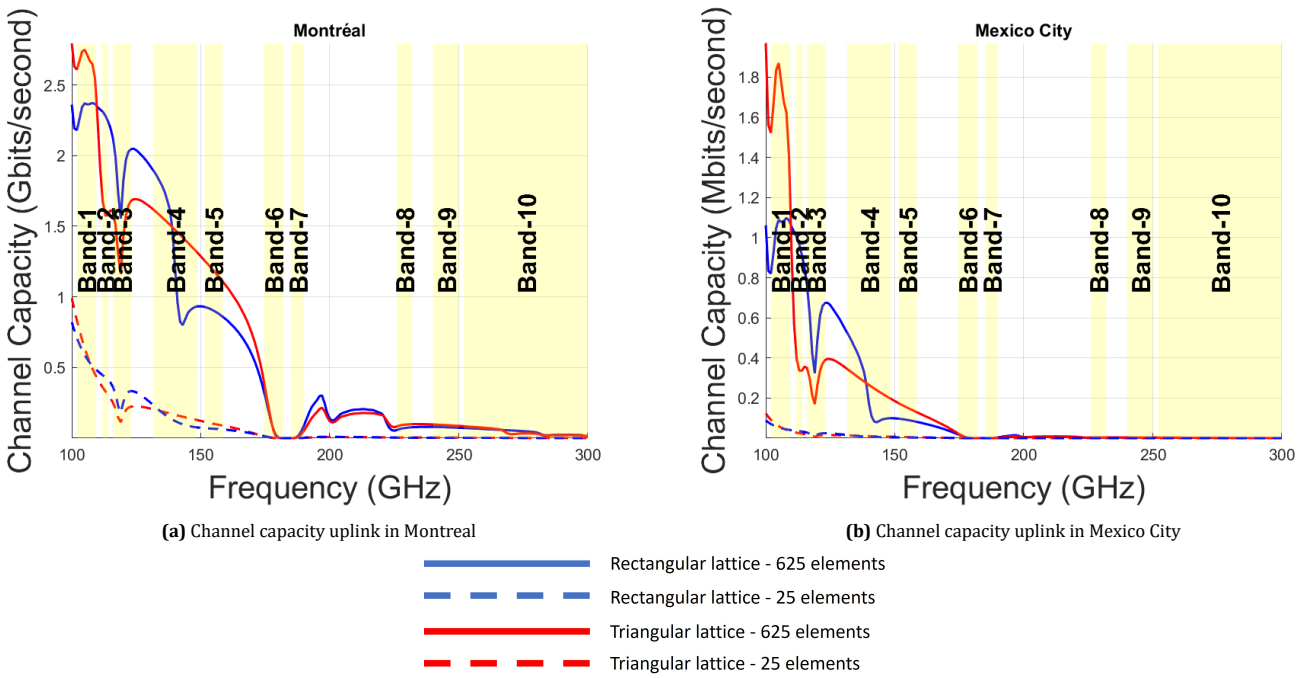

(a) Channel capacity uplink in Montreal

(b) Channel capacity uplink in Mexico City

Fig. 31 – Channel capacity for frequencies between 100 - 300 GHz (500 MHz bandwidth)

ously mentioned, we only considered Montreal and Mexico City due to the zero data rate in Manaos, which persists even with an increased bandwidth. Our analysis indicates that the most substantial performance improvement upon bandwidth increase is observed in Montreal City's uplink, which employs a triangular array of 625 elements, achieving up to 12 Gbits/s. However, for the remaining links in Montreal and Mexico City, we noted that the values are comparable to those obtained using a bandwidth of 500 MHz.

Another option that we considered to enhance the channel capacity in the downlink, is escalate the transmitted power by satellites to the following values: 33.01 dBW, 37 dBW, 40 dBW, and 100 dBW. Also we considered the arrays with the best performance, that are the ones with 625 radiating elements and a bandwidth of 2 GHz. The outcomes of this adjustment are illustrated in figures 33a, 33b and 33c.

These figures illustrate a clear relationship between the augmentation of transmitted power and the enhancement in the channel capacity, namely if we increase the transmitted power, in general, for the three cities we will have higher data rates. The most favourable condition is obtained with a transmission power of 100 dBW, which yields a data rate above 25 Gbits/s for Montreal and above 2.5 Gbits/s for Mexico City. For Manaos, the data rate is still low. Furthermore, we observe a direct correlation between data rate and frequency. In particular, the channel capacity diminishes as the frequency escalates across all cities.

Our results represent a critical scenario because we took into account weather conditions such as rain, fog, clouds and atmospheric gases, all occurring simultaneously. However, under clear, blue sky conditions, we can achieve improved results.

In this context, we also computed the channel capacity for the downlink and uplink, considering only the free-space loss that is show in Fig. 13, a transmitted power of 29 dBW and a bandwidth of 500 MHz. The results are depicted in Fig. 34, where the blue lines correspond to the results for rectangular phase arrays with 625 elements, while the red lines represent rectangular phase arrays with 25 elements. The green lines are associated with triangular phase arrays comprising 625 elements, and the black lines denote triangular phase arrays with 25 elements. Furthermore, solid lines consider the minimum free space attenuation observed at satellites at an altitude of 200 km, while dashed lines consider the maximum free space attenuation observed at satellites at an altitude of 2000 km. It is important to mention that these results are applicable to the three cities under study.

From Fig. 34 we can observe that there exists a direct relationship between the increasing of the frequency and the reduction of the channel capacity. Additionally, the behaviour of the data rate is similar between the different architectures of the antennas.

The best scenario is observed for the communications with satellites that operates at an altitude of 200 km, yielding a maximum data rate of 17.3 Gbits/s. For satellites in an altitude of 2000 km it is possible to reach up to 15.1 Gbits/s.

Upon comparing figures 30, 31 and 34, it becomes evident that weather conditions play a crucial role in determining the data rate achievable in both the downlink and uplink scenarios. This is particularly significant for the downlink due to the power transmission limitations of a LEO satellite.

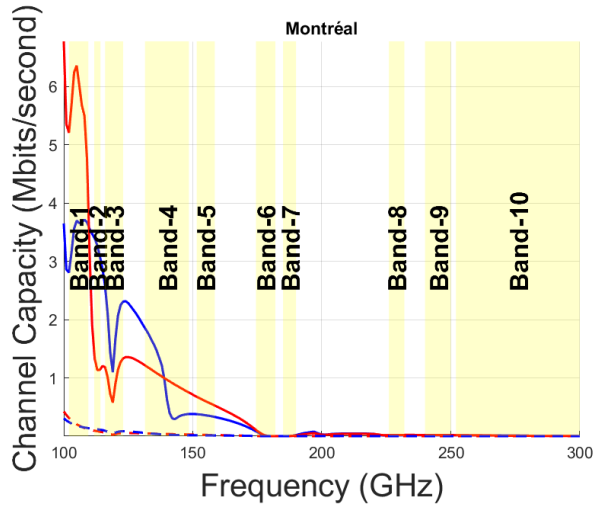

(a) Channel capacity for the downlink in Montreal

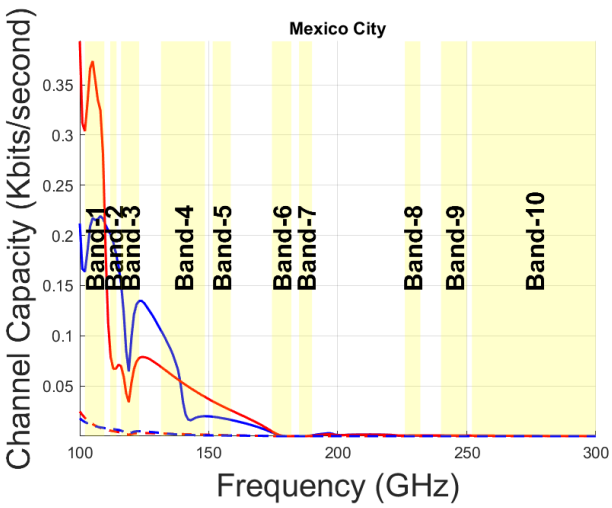

(b) Channel capacity for the downlink in Mexico City

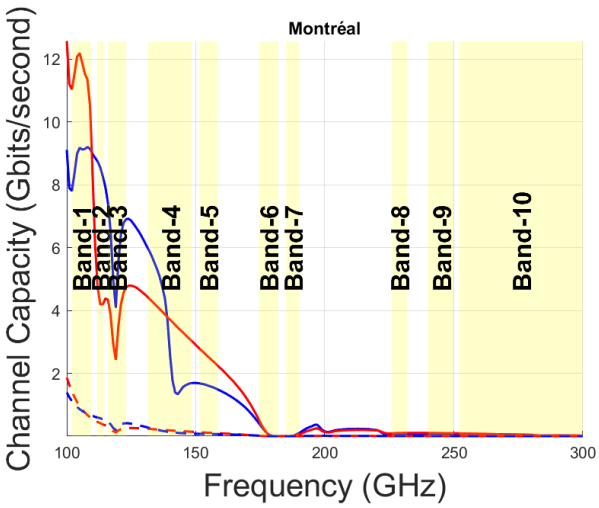

(c) Channel capacity uplink in Montreal

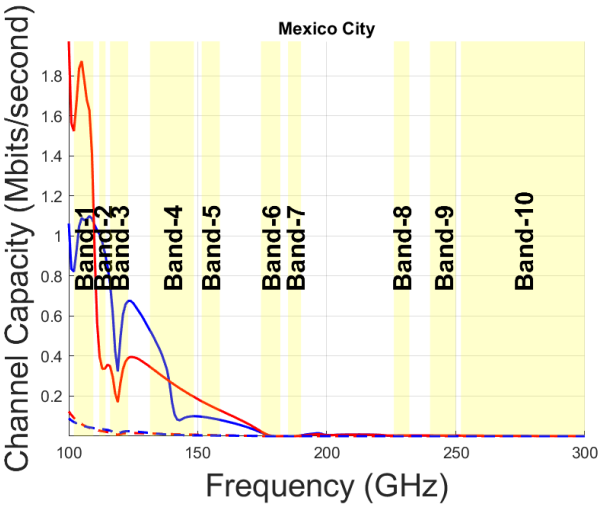

(d) Channel capacity uplink in Mexico City

Fig. 32 – Channel capacity for frequencies between 100 - 300 GHz (5 GHz bandwidth)

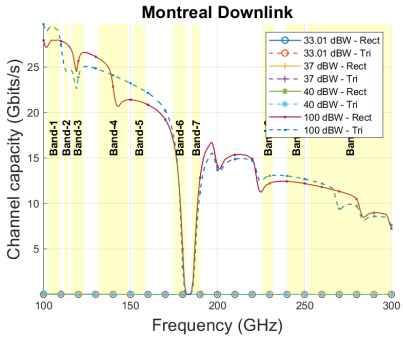

(a) Channel capacity in Montreal

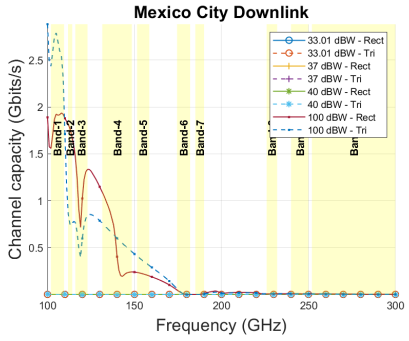

(b) Channel capacity in Mexico City

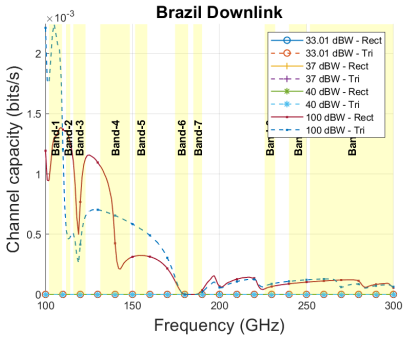

(c) Channel capacity in Manaos

Fig. 33 – Channel capacity in Mexico City for different values of transmitted power

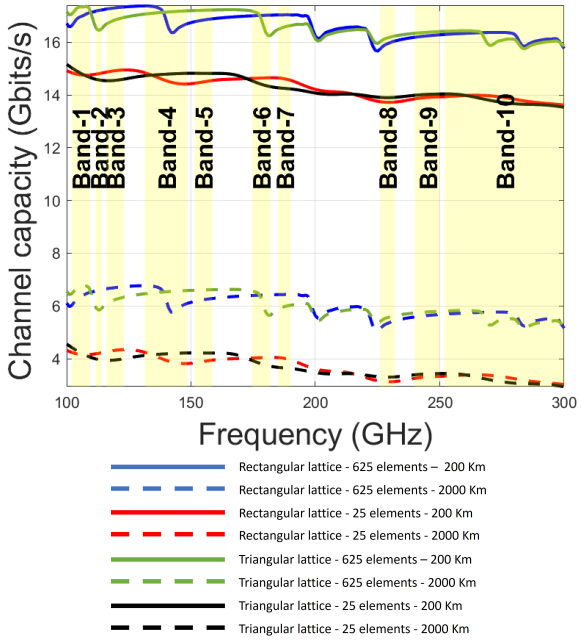

Fig. 34 – Channel capacity for the downlink considering blue sky

4.4.2 Inter-satellite links

Regarding the channel capacity for ISL between satellites in the same orbit, the results are shown in Fig. 35, where the superior sub-figure contemplates the information for the rectangular lattice and in the inferior sub-figure the triangular lattice. Furthermore, the blue lines represent computations for an array consisting of 625 elements, while the red lines correspond to an array with 25 elements. Additionally, we use solid lines to denote the channel capacity in satellites at an altitude of 200 km, dashed lines represent satellites at an altitude of 1000 km, and dash-dotted lines indicate satellites at an altitude of 2000 km.

From Fig. 35 we can see that the channel capacity follows a trend of horizontal peaks and troughs, each manifesting within distinct bands. Additionally, depending on the type of lattice, we can take advantage of all the bands because both of them demonstrate similar values of data rate but in different frequency bands.

From Fig. 35, the maximum data rate is 2.3 Gbits/s, observed in the communication between satellites in the 200 km-orbit equipped with a phase array of 625 elements. In contrast, the minimum values, ranging approximately up to 0.5 Gbits/s, which are associated with antennas comprising 25 radiating elements. Thus, the phase arrays with 625 elements outperform those with 25 elements.

Regarding the channel capacity for ISL between satellites in different orbits, the results are depicted in Fig. 36, where blue lines represent computations for an array consisting of 625 elements, while the red lines correspond to

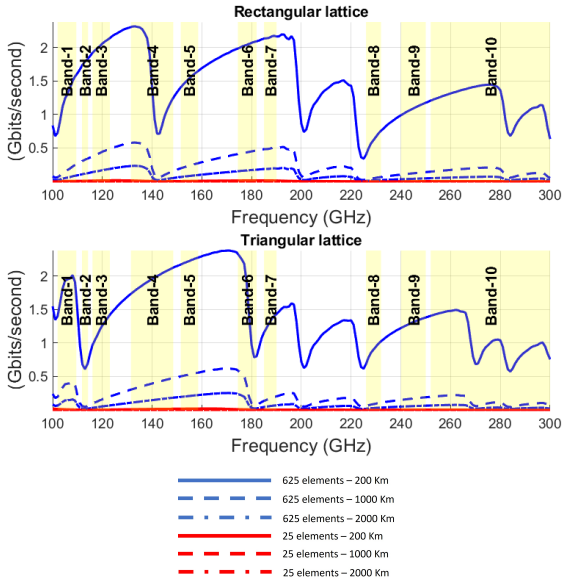

Fig. 35 – ISL channel capacity for frequencies between 100 - 300 GHz

an array with 25 elements. Solid lines are used to indicate the SNR in satellites at an altitude of 200 km, communicating with other satellites at an altitude of 1000 km (800 km of distance). Dashed lines depict satellites at an altitude of 200 km communicating with other satellites at an altitude of 2000 km (1800 km of distance).

From Fig. 36 we can observe that the 625 elements design antenna has a better performance, in comparison with the 25 elements design antenna. For this last one, the channel capacity is approximately zero. Additionally, we noted that the data rate in inter-orbit communications exhibits a behaviour similar to that in same-orbit communications.

In general, for both types of antenna, the channel capacity in ISO ranges between 0.5 Gbits/s and 2 Gbits/s. From these results we noted that the maximum data rate is observed in the communication between satellites at a dis-

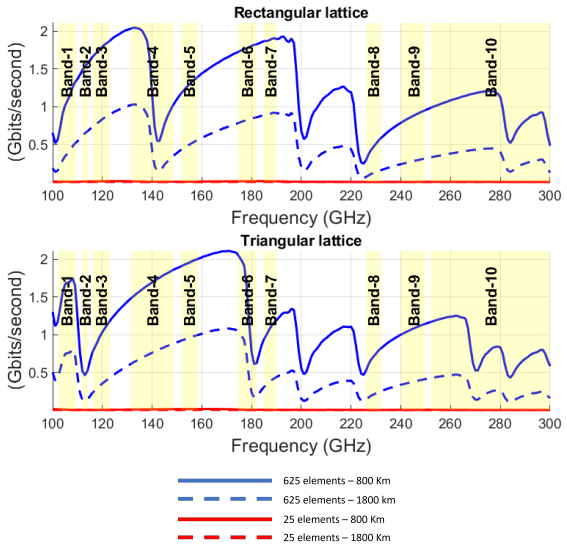

Fig. 36 – ISO channel capacity for frequencies between 100 - 300 GHz

tance of 800 km equipped with a phase array of 625 radiating elements. In contrast, the minimum values correspond to antennas comprising 25 radiating elements.

5. REGULATORY ASPECTS

This section provides an overview of the current regulatory framework in the ITU and the potential regulatory challenges that may arise for the allocation of frequencies under study. The section also discusses the possible strategies and actions to overcome these challenges and to facilitate the harmonization and coordination of the frequencies at the regional and global levels.

5.1 ITU regulatory framework

The United Nations has a specialized agency dedicated to communication technologies and telecommunication, namely, the ITU [40]. According to the provisions of article 1, number 1, paragraphs a) and c) of the ITU Constitution [41], the ITU is the global entity responsible for fostering and extending international collaboration among its member states on telecommunication matters in order to encourage the growth of technology and its most effective use to boost the efficiency of telecommunication services, expand their usage, and make them as widely accessible to the public as possible.

In order to guarantee such principles, the ITU generates and coordinates different instruments, procedures and databases used, among other things, to achieve international coordination of the use and occupation of orbits and their associated frequencies. Furthermore, the ITU is divided in 3 sectors: development of telecommunications, radiocommunications and standardization of the telecommunications.

According to [42], the mission of the ITU Radiocommunication sector (ITU-R) includes ensuring the rational, fair, efficient and economical utilization of the radiofrequency spectrum by all radiocommunication services. This includes those that use satellite orbits. Additionally, this entity manages the allocation of spectrum frequencies and its assignment, maintaining the master international register of frequency assignments. Likewise the ITU-R coordinates efforts to prevent and eliminate harmful interference between the different radiocommunication services globally.

Moreover, the ITU carries out its work through the following conferences and meetings:

- ITU Council
- ITU Plenipotentiary Conference
- Radio Regulations Board (RRB)
- World Radiocommunication Conferences (WRCs);
- Radiocommunication Assemblies (RA)
- World Conference on International Telecommunications (WCIT)
- World Telecommunication Standardization Assembly (WTSA)
- Study Groups
- ad-hoc groups, events, regional and global meetings and workshops;
- World Telecommunication Development Conference (WTDC)

As mentioned before, the ITU-R is the area in charge of fulfilling the objectives of the ITU in wireless communications, including satellite matters. For this purpose, it has the RR, which consists of an international treaty and its objectives are:

- facilitate fair and rational use of frequency spectrum and satellite orbits;
- ensure availability and protection of frequencies for relief and security purposes;
- contribute to prevention and resolution of harmful interference between radiocommunication services;
- facilitate effective and efficient operation of all radiocommunication services;
- consider and regulate new applications of radiocommunication technology, if needed.

In addition to the above points, the RR defines the procedures, standards and duties for all Member States in relation to radiocommunication services. In this context, article 5 of the RR contemplates the Frequency Allocation Table, where the world is divided into three regions (See Fig. 37). Region 1 (R1) comprises Europe and Africa, Region 2 (R2) covers the Americas, and Region 3 (R3) includes Asia and Oceania. The Frequency Allocation Table shows the different radiocommunication services that can be used in each region and frequency. Some services may have the same allocation across regions, but others may vary depending on the region. This means that not all services are globally available, and some may be limited to one or two regions only.

The RR was adopted and continuosly revised by the WRCs, including article 5 of the RR in order to add new allocations for radiocommunication services. The WRCs are international meetings that occur every 3-4 years to review and revise the RR according to an agenda set by the ITU Council based on recommendations from previous conferences.

WRC has the authority to revise associated frequency assignment plans, address global radiocommunication issues, oversee the Radio Regulations Board and the Radiocommunication Bureau, and set study questions for the Radiocommunication Assembly and its Study Groups for future conferences [43].

Regarding the agenda for each WRC, the Conference Preparatory Meeting (CPM) prepares a consolidated report based on contributions from countries, Study

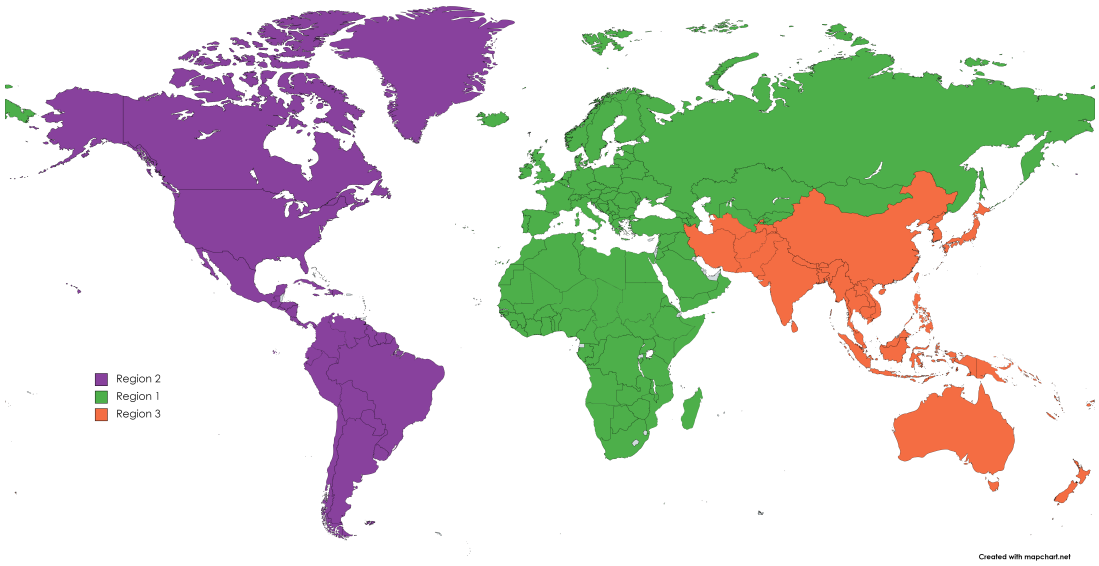

Fig. 37 – ITU regions. *Image created with MapChart*

Groups, and other sources such as academia and industry. This report provides technical and regulatory arguments, as well different methods to solve each of the agenda items, according to the results of the studies carried out during the study cycle. The CPM report is proposed for consideration for the work of WRCs.

In order to take decisions at the WRC, agreements between regions and countries should be reached. In this regard, as preparation of the discussions at the WRC level, there are some other international meetings at regional levels. For example, to get a regional position in R2, the WRC agenda items are discussed at the Inter-American Telecommunication Commission (CITEL), which consists of the official technical advisors of the Organization of American States in telecommunications, information and communication technologies. The main objective of CITEL is "*to facilitate infrastructure deployment and telecommunication service delivery; harmonization of the radio frequency spectrum to reduce the cost of providing wireless services; information and communication technology (ICT) training; or helping countries devise telecommunication development strategies*" in R2 [44].

In addition to CITEL, there are other regional organizations that deal with telecommunication issues, such as the African Telecommunication Union (ATU), Asia-Pacific Telecommunity (APT), Arab Information and Communication Technologies Organization (AICTO), Regional Commonwealth in the field of Communications (RCC) and others [45].

Furthermore, some countries have their own forums where they can develop their positions based on the input of their industry, academia and public entities. This allows them to make informed decisions that suit their needs and interests.

An example of this is Mexico, which has the Technical Committee on Radio Spectrum Matters (CTER) of the Federal Telecommucications Institute. The CTER is a dedicated technical support committee in the radio spectrum domain, serving in an advisory capacity without any obligatory powers. It showcases the present and prospective needs of the radio spectrum for all types of radiocommunication services, inclusive of the spectrum required for satellite communications [46].

5.2 Process for the adoption of 100 - 300 GHz band

Considering the context previously described, as part of this investigation we explore the viability of the regulatory implementation of our research, taking into account the ITU process to allocate frequencies bands (see Fig. 38).

Focusing on the new satellite allocations, first it is necessary to generate a national position, where usually academia and industry can support by providing technical documents about the viability of adopting new allocations for satellite services in the frequency bands 100-300 GHz, considering topics such a need for more spectrum, channel propagation and possibility of harmful interference to other radiocomunication services or economic perspectives.

The national contributions may considers technical inputs that could be beneficial to the ITU Study Groups or for the conference preparatory meetings. If a country has a preliminary viewpoint or a preliminary proposal regarding the agenda items for the WRC, it can be submitted to the regional entity to which the country belongs. For Brazil, Canada and Mexico, their national positions should be submitted to CITEL. At regional meetings, these positions will be presented, discussed, and the authors will attempt to gain support from other countries in the region. Once a preliminary proposal receives support from

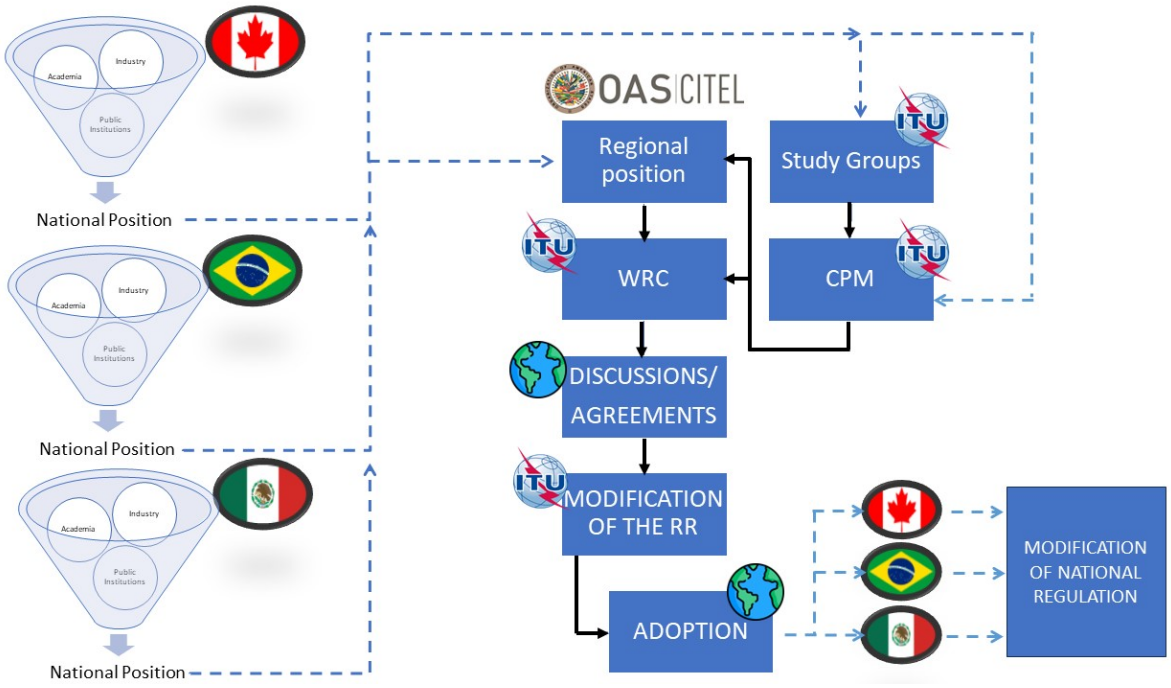

Fig. 38 – Regulatory process to adopt new frequency allocations

more than two countries, it becomes a draft of an Inter-American Proposal. If it gains support from more than four countries, it becomes an Inter-American Proposal (IAP). This IAP can be submitted to the WRC as the position of Region 2. However, if a country in any region disagrees with its region's position, it can directly send a contribution to the WRC as a national position.

During the WRC, all regions and countries are required to discuss, negotiate and reach agreements or compromises regarding the adoption of new or revised technical regulations, standards and procedures. At the conclusion of the conference, the ITU publishes the acts of the WRC, which display the results and serve as the baseline for subsequent modifications to the RR. These modifications are typically published at least one year after the respective WRC. However, the majority of the WRC's changes become valid the day after the conference concludes.

As part of the global adoption, not only do industry players have to develop new equipment or telecommunication structures that comply with the RR, but governments also have to adjust their national regulations accordingly. This means updating their national Frequency Allocation Table to reflect the changes in the RR and ensure a harmonized use of the spectrum.

5.3 Regulatory challenges

- **Time of implementation.** Taking into account the process outlined in Fig. 38, the implementation of a new allocation, from inception to the point where satellites operate within these new allocations, could be a lengthy process. This is primarily due to the regulatory process.

  An idea needs to be proposed at one WRC and it may be approved for study at the following WRC. The study cycle then commences and concludes three or four years later. Once the new allocations are approved, they become official with the publication of the new version of the RR, which occurs one year after the WRC.

  Subsequently, all countries are required to modify their national regulatory frameworks to align it with these changes. During this period, the industry can also begin to manufacture new equipment or submit the respective satellite filings to the ITU.

  In summary, this entire process could take a minimum of eight years to materialize. However, it's important to note that any modification to the RR undergoes a similar timeline.

- **Adoption.** Considering that different countries and regions may have different spectrum policies, priorities and preferences, which can create conflicts and inconsistencies when allocating new frequencies, by making frequencies between 100 GHz and 300 GHz available for use by satellite services in each country, new national regulatory procedures, licensing conditions, fees and other processes will appear. However, we believe that this challenge is already being mitigated because satellite companies have a lot of experience addressing national regulatory requirements for spectrum access. As such the existing regulatory burden is not expected to be worse at THz frequencies than it is already at lower frequencies.

- **Protection to incumbent services.** Another regula-

tory challenge to adopt new frequency allocations to balance the needs of existing and new services. Existing services have already been assigned or authorized to use certain frequencies for specific purposes and they may have invested heavily in infrastructure and equipment that relies on that spectrum. Regulators need to ensure that new frequency allocations do not disrupt incumbent services, while also creating opportunities for new services to emerge.

Regulators can balance the needs of existing and new services by imposing technical or operational conditions on spectrum use, such as limiting power output, restricting geographic coverage or requiring sharing arrangements. They can also use market-based mechanisms, such as auctions, fees or trading, to allocate spectrum efficiently and fairly among different users.

6. PROJECT ASSESSMENT

This section provides an analysis of the global prospects of the THz frequencies proposed in this study, considering the scalability of their implementation, risk level, social impact and the anticipated challenges.

6.1 Scalability

With the frequencies identified in this research it is expected to augment the capabilities of the LEO mega-constellations, taking advantage of the existing scalability and global reach is intrinsic to their design. However, having access to more spectrum for these systems, will enable more of these satellite systems to exist and compete as spectrum availability will no long play the limiting role it has today. This will help in a limited manner to scale up services and reduce prices, thereby benefiting more people and potentially eliminating the digital divide.

While THz frequencies could also be used by Geo-synchronous Orbit (GEO) satellite systems, the intrinsic advantages of LEO systems which naturally provide for more frequency reuse, global reach and significantly lower latency, make the LEO systems better candidates for our solution.

6.2 Risk level

Overall, the risk assessment of our solution is low risk, with a high likelihood of return. One of the risks identified is that no regulatory framework has been developed for satellite services in the frequency bands under study. However, this risk is mitigated by the high level of industry/government interest and the current work on building a regulatory framework for THz bands, which has already begun.

6.3 Social impact

The identification of additional spectrum will allow LEO mega-constellation satellite operators to offer higher speed broadband services around the globe. This means that citizens everywhere, even in remote areas, would be able to enjoy fibre-like speeds in low latency Internet access areas. The benefits of Internet access are well known and underpin the digital economy. For example, the World Bank indicates that in developed countries, as is shown in [47], if Internet penetration rises by 10%, GDP rises by 1.19% and in developing countries, the increase in GDP is 1.35%. The availability of a more reusable spectrum with higher speeds is expected to increase capacity and drive down the cost of the service. This is a normal part the economics around pricing, although the ability of individual markets to bear a certain price is likely to be the ultimate driver.

This project has the potential to eliminate the digital divide, making available satellite services to encourage healthcare, education, employment and agriculture even in rural areas. For example, Deloitte´s study of 2021 [48] shows that a 10 Mbps increase in average download speeds would have resulted in 139,400 additional jobs in a period of 3 years. They also show that going from dial-up speeds to broadband speeds has a much larger direct impact on economic growth, especially in rural areas.

Furthemore, the COVID-19 pandemic boosted Internet access overall by encouraging more people to go online for work or play, but in some countries it exacerbated existing digital divides between and within countries related to age, disability, gender, geography and socioeconomic status. With many essential services pushed online, there is a real and present danger that those without broadband Internet access could be left even further behind [49].

As our solution has the potential to help eliminate the digital divide, the benefits of better connectivity and full participation in the digital economy benefits all users equally. However, these benefits have the potential to be more meaningful for contributing to the inclusion of people in underserved user communities because these areas will experience the largest increase in effective connectivity levels.

6.4 Anticipated challenges

One of the anticipated challenges is the technological maturity of radio front ends capable of operating at THz frequencies because the implementation of our solution depends on the equipment available. The wireless equipment that already operates in THz bands is expensive and they are either in an early stage of development or just starting to become available. However, given the high level of industry interest, it is expected that equipment availability will increase significantly during the time frame of our project (2-4 years).

Another challenge that we consider is related to market access, which refers to the capability of satellite operators

to offer services in different countries. By making the THz band available for use by satellite services in each country, new national regulatory procedures, licensing conditions, fees and other processes will appear. However, we believe that this challenge is already being mitigated because satellite companies have a lot of experience addressing national regulatory requirements for spectrum access. As such the existing regulatory burden is not expected to be worse at THz frequencies than it is already at lower frequencies.

7. CONCLUSION

A non-terrestrial system that consists of three layers: a top layer of LEO satellites, a middle layer of aeronautical ESIMs and a lower layer of Earth stations on the Earth's surface, is presented. This non-terrestrial network was designed to operate in some frequency bands between 100 and 300 GHz, which are being considered by the ITU and Canada for future development of wireless communications. We also evaluate the impact of signal propagation attenuation through different links: ESIM-to-satellite, satellite-to-Earth station, inter-satellite link in the same orbit and inter-satellite link in different orbits and vice versa.
Results show that:

- The frequency bands between 102 - 109.5 GHz are ideal for communication between Earth stations and satellites and vice versa. These results also are applicable to communication with ESIMs on an aircraft; this is because the altitude difference between an Earth station on land and one aboard an aircraft is negligible (around tens of kilometers), especially when compared to the distance to LEO satellites, which are hundreds or even thousands of kilometers away.

  In a critical scenario with simultaneous weather effects such as rain, fog, cloud and atmospheric gases, Band-1 can achieve data rates of up to 2.6 Gbits/s with 0.5 GHz of bandwidth or up to 12 Gbits/s with 5 GHz of bandwidth in the uplink. For the downlink, we can reach up to 6 Mbits/s considering $p_{tx} = 29$ dBW, in cities like Montreal or 350 Mbits/s in locations like Mexico City. However, by increasing the power up to 100 dBW and considering a bandwidth of 2 GHz, we can reach 25 Gbits/s in Montreal and 2.5 Gbits/s in Mexico City. It is important to note that the data rate of the downlink is contingent on the satellite's power transmission capabilities. Data for Manaos is excluded due to its negligible values, attributable to the city's low SNR.

  However, under clear, blue sky conditions, we can achieve improved results. For instance, the best scenario is observed that in Band-1 for communication with satellites operating at an altitude of 200 km, yielding a maximum data rate of 17.3 Gbits/s. For satellites at an altitude of 2000 km, it is possible to reach up to 15.1 Gbits/s. This information is applicable for all the cities under study.

  Moreover, in order to increase the performance of the downlink and uplink in a critical scenario, we additionally could increase the gain of the phase array raising the number of its elements. This option could be more affordable than increasing the power. This result is a potential study for the future.

- The frequency bands between 111.8 – 114.25 GHz, 116 – 123 GHz, 174.5 – 182 GHz and 185 – 190 GHz, present viable options for inter-satellite links ,specifically for communication between satellites in the same orbit. These bands can deliver speeds from 1.5 to 2.51 Gbits/s when utilizing a uniform rectangular array with 625 radiating elements. It is important to note that for these types of communications, a rectangular lattice is preferred due to the significantly lower data rates of the triangular lattice.

- The frequency bands between 111.8 – 114.25 GHz, 116 – 123 GHz, 174.5 – 182 GHz and 185 – 190 GHz are ideal for facilitating communication between satellites in different orbits. Utilizing a uniform rectangular array with 625 radiating elements, these bands can achieve data transfer rates ranging from 0.5 Gbits/s to 2 Gbits/s. It is important to note that for these types of communications, a rectangular lattice is preferred as the triangular lattice has significantly lower data rates compared to the rectangular lattice.

- Furthermore, it is crucial to understand the environment in which the Earth station operates as the weather conditions affect greatly the attenuation. This allows us to account for any signal propagation attenuation. We conducted an analysis of three cities, each with a distinct weather profile. As expected, our observations indicated that in regions classified as heavy rain areas, the signal attenuation was significantly high.

- In the process of new satellite allocations, a national position is first established, often supported by academia and industry through technical documents. In this case, our research can be an input for national contributions as benefit to the ITU Study Groups or conference preparatory meetings.

  After that, preliminary viewpoints or proposals regarding the WRC agenda items can be submitted to the respective regional entity. For Brazil, Canada and Mexico, these should be submitted to CITEL. At regional meetings, these positions are presented, discussed and support is sought from other countries in the region.

  During the WRC, all regions and countries discuss, negotiate and reach agreements or compromises regarding the adoption of new or revised technical regulations, standards and procedures. In this case, it

could be the new allocations for satellite services in THz. After that, the ITU publishes the acts of the WRC at the conclusion of the conference, displaying the results and serving as the baseline for subsequent modifications to the RR. These modifications are typically published at least one year after the respective WRC, but the majority of the WRC's changes become valid the day after the conference concludes.

As part of the global adoption, industry players must develop new equipment or telecommunication structures that comply with the RR and governments must adjust their national regulations accordingly. This includes updating their national Frequency Allocation Table to reflect the changes in the RR and ensure a harmonized use of the spectrum.

While this research does not represent a new discovery, it does offer fresh results derived from applying the synthesis of approaches found in the existing literature. These fresh results are therefore valuable for the future allocation of the most suitable frequencies between 100 - 300 GHz to satellite services.

7.1 Open issues

Regarding our results, in future research, the following topics have the potential to be explored for THz frequencies.

- *Misalignment*. This research investigated the attenuation of signals and its impact on communication quality. However, attenuation is not the only factor that can degrade the signal; another one is the misalignment between the transmitter and receiver antennas. This research started to explore the misalignment effects for frequencies ranging from 100 to 300 GHz. However, further research is required to gain a deeper understanding of satellite communications for these frequencies.

- *Testbed of the sub-THz communication system*. Testing the communication system described in this research, with special software and hardware that operates in THz bands. For example, using the hardware that Poly-Grames acquired in 2022, which includes frequency up and down millimeter-wave compact frequency converter modules, which can be used with signal generators and spectrum analyzers. According to the manufacturer, the Up and Down converter modules "achieve low conversion loss and excellent noise figure" [50], which is beneficial for having more realistic results.

  The testbeds will help us to determine the viability of implementation of antennas such as those described in this article. When experiments would take place it is important to consider the narrow beams that we can obtain at sub-THz frequencies, and the requirements for beam searching, beam tracking, and channel estimation.

- *Frequency bands use in space*. Considering that space communication systems will play a key role in future human exploration of the Moon and Mars. As part of future work, the feasibility of implementing the frequency bands identified in this research for use in communications from the Moon or Mars could be explored.

- *Dynamic spectrum management*. Routing algorithms for THz satellite constellations remain an unexplored area of research. A DSM framework could autonomously determine the optimal frequency for each satellite in a LEO constellation. The DSM algorithm could use Artificial Intelligence (AI) to learn channel characteristics and behaviour, and satellites in a mega-constellation could cooperate by sharing environmental data. This could improve signal performance by optimizing the transmission frequency, thereby increasing the SNR and reducing harmful interference.

- *Constellation scale*. In this article we analyzed the communication between a satellite and an Earth-station, considering a fixed angle of elevation. In this regard potential future research is considering different values of elevation angles. Additionally, it is important to consider, for example the number of satellites in the constellation, their position in the orbital planes and the coverage area.

ACKNOWLEDGEMENT

This research article is funded by NSERC Discovery Grant RGPIN-2022-03355.

REFERENCES

[1] Nasir Saeed, Ahmed Elzanaty, Heba Almorad, Hayssam Dahrouj, Tareq Y. Al-Naffouri, and Mohamed-Slim Alouini. "CubeSat Communications: Recent Advances and Future Challenges". In: *IEEE Communications Surveys Tutorials* 22.3 (2020), pp. 1839–1862. DOI: 10.1109/COMST.2020.2990499.

[2] FCC. *FCC 22-91*. Order and Authorization , Federal Communications Commission, Washington, DC, USA. Washington, DC: USA, Jan. 2022 [online]. URL: https://docs.fcc.gov/public/attachments/FCC-22-91A1.pdf.

[3] ITU-R. *2022 Annual Space Services Report to the STSC 2022 Session on the use of the Geostationary-Satellite Orbit (GSO) and other orbits*. Report. Geneva: International Telecommunication Union, Jan. 2022.

[4] International Telecommunication Union. *Radio Regulations*. http://handle.itu.int/11.1002/pub/814b0c44-en. 2020.

[5] Theodore S. Rappaport, Yunchou Xing, Ojas Kanhere, Shihao Ju, Arjuna Madanayake, Soumyajit Mandal, Ahmed Alkhateeb, and Georgios C. Trichopoulos. "Wireless Communications and Applications Above 100 GHz: Opportunities and Challenges for 6G and Beyond". In: *IEEE Access* 7 (2019), pp. 78729–78757. DOI: 10.1109/ACCESS.2019.2921522.

[6] ITU-R. *Specific attenuation model for rain for use in prediction method*. Recommendation P.838-3. International Telecommunication Union (ITU), 2005. URL: https://www.itu.int/dms_pubrec/itu-r/rec/p/R-REC-P.838-3-200503-I!!PDF-S.pdf.

[7] ITU-R. *Attenuation due to clouds and fog*. Recommendation P.840-8. Working Party 5D, 2022. URL: https://www.itu.int/dms_pubrec/itu-r/rec/p/R-REC-P.840-8-201908-I!!PDF-E.pdf.

[8] H.J. Liebe, T. Manabe, and G.A. Hufford. "Millimeter-wave attenuation and delay rates due to fog/cloud conditions". In: *IEEE Transactions on Antennas and Propagation* 37.12 (1989), pp. 1617–1612. DOI: 10.1109/8.45106.

[9] ITU-R. *Attenuation by atmospheric gases and related effects*. Recommendation P.676-13. International Telecommunication Union (ITU), 2022. URL: https://www.itu.int/dms_pubrec/itu-r/rec/p/R-REC-P.676-13-202208-I!!PDF-E.pdf.

[10] ITU-R. *Draft new Report ITU-R M.[IMT.FUTURE TECHNOLOGY TRENDS OF TERRESTRIAL IMT SYSTEMS TOWARDS 2030 AND BEYOND] - Future Technology Trends of Terrestrial IMT Systems towards 2030 and beyond*. Draft new Report. International Telecommunication Union (ITU), 2022. URL: https://www.itu.int/md/R19-SG05-C-0085/en.

[11] Government of Canada. *Decision on the Technical and Policy Framework for the Frequency Bands Above 95 GHz*. https://ised-isde.canada.ca/site/spectrum-management-telecommunications/en/learn-more/key-documents/decision-technical-and-policy-framework-frequency-bands-above-95-ghz. Accessed: Sep. 02, 2023. 2022.

[12] ITU-R. *Sharing between stations in the fixed service and satellite services in the frequency bands 71-76 GHz and 81-86 GHz*. Resolution 775 (WRC-19). International Telecommunication Union (ITU), 2019. URL: https://www.itu.int/dms_pub/itu-r/oth/0c/0a/R0C0A00000D0032PDFE.pdf.

[13] ITU-R. *Preliminary agenda for the 2027 World Radiocommunication Conference*. Resolution 812 (WRC-19). International Telecommunication Union (ITU), 2019. URL: https://www.itu.int/dms_pub/itu-r/oth/0C/0A/R0C0A00000F00175PDFE.pdf.

[14] Mohammad Ehatasham Shawon, Mostafa Zaman Chowdhury, Md Biplob Hossen, Md Faisal Ahmed, and Yeong Min Jang. "Rain Attenuation Characterization for 6G Terahertz Wireless Communication". In: *2021 International Conference on Artificial Intelligence in Information and Communication (ICAIIC)*. 2021, pp. 416–420. DOI: 10.1109/ICAIIC51459.2021.9415196.

[15] Hitesh Singh, Vivek Kumar, Kumud Saxena, Boncho Bonev, and Ramjee Prasad. "Prediction of Radio Wave Attenuation due to Cloud Using Machine Learning Techniques". In: *2021 56th International Scientific Conference on Information, Communication and Energy Systems and Technologies (ICEST)*. 2021, pp. 163–166. DOI: 10.1109/ICEST52640.2021.9483524.

[16] Hitesh Singh, Vivek Kumar, Kumud Saxena, Vinod M Kapse, Boncho Bonev, and Ramjee Prasad. "Smart Channel Modelling for Cloud and Fog Attenuation Using ML for Designing of 6G Networks at D and G Bands". In: *Wireless Personal Communications* 129.3 (2023), pp. 1669–1692.

[17] Gustavo A. Siles, Jose Manuel Riera, and Padro Garcia-del-Pino. "Atmospheric Attenuation in Wireless Communication Systems at Millimeter and THz Frequencies [Wireless Corner]". In: *IEEE Antennas and Propagation Magazine* 57.1 (2015), pp. 48–61. DOI: 10.1109/MAP.2015.2401796.

[18] Ali J. Alqaraghuli, Hussam Abdellatif, and Josep M. Jornet. "Performance Analysis of a Dual Terahertz/Ka Band Communication System for Satellite Mega-Constellations". In: *2021 IEEE 22nd International Symposium on a World of Wireless, Mobile and Multimedia Networks (WoWMoM)*. 2021, pp. 316–322. DOI: 10.1109/WoWMoM51794.2021.00058.

[19] Shanyun Liu, Xianbin Yu, Rongbin Guo, Yajie Tang, and Zhifeng Zhao. "THz channel modeling: Consolidating the road to THz communications". In: *China Communications* 18.5 (2021), pp. 33–49. DOI: 10.23919/JCC.2021.05.003.

[20] ITU-R. *Calculation of free-space attenuation*. Recommendation P.525-4. International Telecommunication Union (ITU), 2019. URL: https://www.itu.int/dms_pubrec/itu-r/rec/p/R-REC-P.525-4-201908-I!!PDF-E.pdf.

[21] Shuai Nie and Ian F. Akyildiz. "Channel Modeling and Analysis of Inter-Small-Satellite Links in Terahertz Band Space Networks". In: *IEEE Transactions on Communications* 69.12 (2021), pp. 8585–8599. DOI: 10.1109/TCOMM.2021.3113942.

[22] ITU-R. *A milestone-based approach for the implementation of frequency assignments to space stations in a non-geostationary-satellite system in specific frequency bands and services*. Resolution 35 (WRC-19). International Telecommunication Union (ITU), 2019. URL: https://www.itu.int/en/ITU-R/space/Documents/RES35(WRC-19).pdf.

[23] ITU-R. *Agenda for the 2023 World Radiocommunication Conference*. Resolution 811 (WRC-19). International Telecommunication Union (ITU), 2019. URL: https://www.itu.int/dms_pub/itu-r/oth/0c/0a/R0C0A00000D0041PDFE.pdf.

[24] I.T. Union. *Handbook on Earth Exploration-Satellite Service*. United Nations Fund for Population Activities, 2017. ISBN: 9789261189617. URL: https://books.google.ca/books?id=wg4BEAAAQBAJ.

[25] Transfinite Systems. *WRC 2027 Agenda Item Details*. https://www.transfinite.com/content/wrc2027list. Accessed on 2024-03-03. 2023.

[26] National Centers for Environmental Information. *Global Summary of the Month*. https://www.ncei.noaa.gov/access/search/data-search/global-summary-of-the-month. Accessed on 2023-09-01. 2021.

[27] Engineering-ToolBox. *Moist Air - Water Vapor and Saturation Pressure*. https://https://www.engineeringtoolbox.com/water-vapor-saturation-pressure-air-d_689.html. Accessed: [4/8/2023].

[28] ITU-R. *Characteristics of precipitation for propagation modelling*. Recommendation P.837-7. International Telecommunication Union (ITU), June 2017. URL: https://www.itu.int/dms_pubrec/itu-r/rec/p/R-REC-P.837-7-201706-I!!PDF-E.pdf.

[29] Alexander G. Cherevko and Yury V. Morgachev. "Simulation of phased array in THz region". In: *2016 13th International Scientific-Technical Conference on Actual Problems of Electronics Instrument Engineering (APEIE)*. Vol. 02. 2016, pp. 193–199. DOI: 10.1109/APEIE.2016.7806447.

[30] ITU-R. *Rain height model for prediction methods*. Recommendation P.839-3. International Telecommunication Union (ITU), 2001. URL: https://www.itu.int/dms_pubrec/itu-r/rec/p/R-REC-P.839-3-200102-S!!PDF-E.pdf.

[31] I.T. Union. *ITU Handbook on Satellite Communications*. Wiley, 2002. ISBN: 9780471221883. URL: https://books.google.ca/books?id=Qu8KAAAACAAJ.

[32] ITU-R. *Propagation data and prediction methods required for the design of Earth-space telecommunication systems*. Recommendation P.618-14. International Telecommunication Union (ITU), 2023. URL: https://www.itu.int/dms_pubrec/itu-r/rec/p/R-REC-P.618-14-202308-I!!PDF-E.pdf.

[33] Zhenwei Zhao and Zhensen Wu. "Millimeter-wave attenuation due to fog and clouds". In: *International Journal of infrared and millimeter waves* 21.10 (2000), pp. 1607–1615.

[34] American Meteorological Society. *Extinction cross section*. Accessed on September 10, 2023. 2022. URL: https://glossary.ametsoc.org/wiki/Extinction_cross_section.

[35] ITU-R. *The radio refractive index: its formula and refractivity data*. Recommendation P.453-4. International Telecommunication Union (ITU), 2019. URL: https://www.itu.int/dms_pubrec/itu-r/rec/p/R-REC-P.453-14-201908-I!!PDF-E.pdf.

[36] Shkelzen Cakaj. *Ground Station Design and Analysis for LEO Satellites: Analytical, Experimental and Simulation Approach*. John Wiley & Sons, 2022.

[37] T.M. Braun and W.R. Braun. *Satellite Communications Payload and System*. IEEE Press. Wiley, 2021. ISBN: 9781119384328. URL: %5Curl%7Bhttps://books.google.com.mx/books?id=nHc5EAAAQBAJ%7D.

[38] Kyle Reis. "Modulation Schemes, Coding Rates, and 4G/5G Data Speeds". In: *Waveform* (2023). Accessed on 2023-09-17. URL: https://www.waveform.com/a/b/guides/modulation-coding-speeds.

[39] Giovanni E Corazza. *Digital satellite communications*. Springer Science Business Media, 2007.

[40] ITU. *About International Telecommunication Union (ITU)*. https://www.itu.int/en/about/Pages/default.aspx. Accessed on 2023-10-01.

[41] International Telecommunication Union (ITU). *Constitution of the International Telecommunication Union*. Accessed: 2023-11-01. 2023. URL: https://www.itu.int/en/council/Documents/basic-texts/Constitution-E.pdf.

[42] ITU-R. *Mission statement*. https://www.itu.int/en/ITU-R/information/Pages/mission-statement.aspx. Accessed on 2023-10-01.

[43] *World Radiocommunication Conferences (WRC)*. https://www.itu.int/en/ITU-R/conferences/wrc/Pages/default.aspx. Accessed on 2023-10-25.

[44] Inter-American Telecommunication Commission (CITEL). *About - Inter-American Telecommunication Commission (CITEL)*. Accessed: 2023-11-01. 2023. URL: https://www.oas.org/ext/en/main/oas/our-structure/agencies-and-entities/citel/About/Details/category/citel/about-citel.

[45] International Telecommunication Union (ITU). *ITU-T Regional Groups*. Accessed: 2023-11-01. 2023. URL: https://www.itu.int/en/ITU-T/regionalgroups/Pages/default.aspx.

[46] Instituto Federal de Telecomunicaciones (IFT). *Marco de Referencia del Espectro Radioeléctrico*. Accessed: 2023-11-01. 2023. URL: https://www.ift.org.mx/espectro-radioelectrico/marco-de-referencia.

[47] Viasat. *The economic benefits of digital inclusion*. https://news.viasat.com/blog/corporate/the-economic-benefits-of-digital-inclusion. Accessed: Aug. 02, 2023. 2019.

[48] Deloitte. *Deloitte: Quantifying the Economic Impact of Closing the Digital Divide*. https://www2.deloitte.com/us/en/pages/about-deloitte/articles/press-releases/quantifying-the-economic-impact-of-closing-the-digital-divide.html. Accessed: Aug. 02, 2023. 2021.

[49] ITU. *Digital inclusion of all*. https://www.itu.int/en/mediacentre/backgrounders/Pages/digital-inclusion-of-all.aspx. Accessed: Aug. 02, 2023. 2022.

[50] *Keysight Series N5700 User's Guide*. Keysight Technologies. 2021. URL: https://www.keysight.com/ca/en/assets/9018-04515/user-manuals/9018-04515.pdf?success=true.

AUTHORS

Estephania Flores Aguilar received a B.S. degree in telecommunication engineering from the National Autonomous University of Mexico, Mexico City, Mexico, in 2017. She received a master's degree in electrical engineering from Polytechnique Montreal in early 2024. Her current research topics are terahertz-frequency used by non-geostationary satellites. Estephania began her professional career in 2016 with the telecommunication regulator of Mexico, where she specialized in the domestic and international regulation of satellite communications.

Gunes Karabulut Kurt is currently an associate professor of electrical engineering at Polytechnique Montréal, Montreal, QC, Canada. She is a Marie Curie Fellow and received the Turkish Academy of Sciences Outstanding Young Scientist (TÜBAGEBIP) Award in 2019. In addition, she is an adjunct research professor at Carleton University. She is a member of the IEEE WCNC Steering Board. She is the chair of the IEEE special interest group entitled "Satellite Mega-constellations: Communications and Networking." Her research interests include space information networks, satellite networking, wireless network coding, wireless security and space security.